Article

Molecular Cell

# Activation of bacterial programmed cell death by phage inhibitors of host immunity

## Graphical abstract

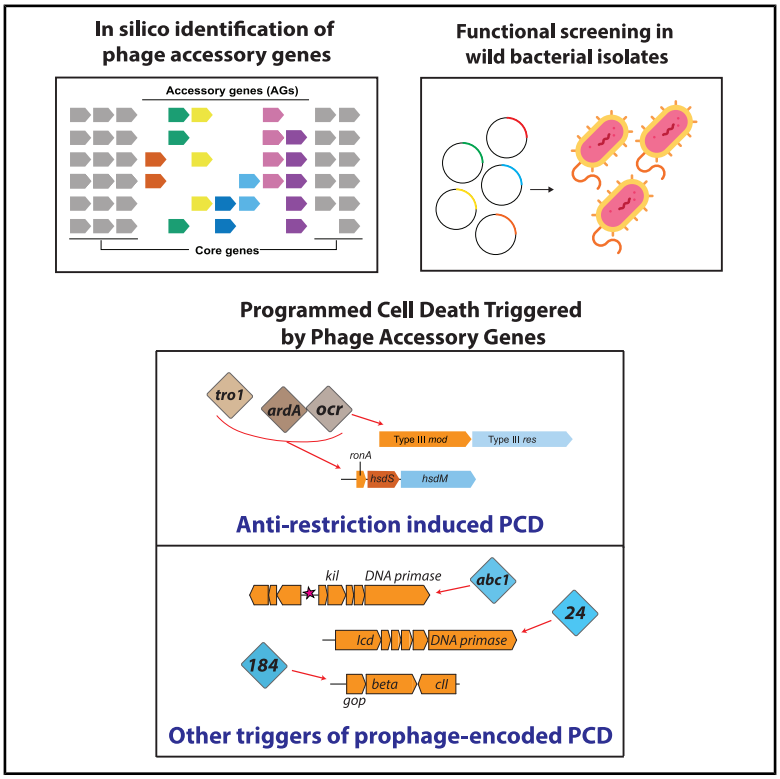


## Highlights

- Platform identifies AGs from phage genomes and assigns functions to them
- AGs triggered programmed cell death activity of "decoy" and "self-guarded" R-M systems
- Multiple AGs can be recognized by the same defense systems
- Counter-defense AGs activate abortive infection systems found in prophages

## Authors

Sukrit Silas, Héloïse Carion, Kira S. Makarova, ..., Franklin L. Nobrega, Eugene V. Koonin, Joseph Bondy-Denomy

## Correspondence

sukrit.silas@gladstone.ucsf.edu (S.S.), joseph.bondy-denomy@ucsf.edu (J.B.-D.)

## In brief

Silas et al. have designed a pipeline to identify accessory genes (AGs) computationally from thousands of phage genomes at once, and they built a screening platform to assay their functions in many wild strains of bacteria in parallel. They find that counter-defense AGs can elicit programmed cell death (PCD) responses from restriction-modification systems, the most common antivirus defenses in bacteria.

Silas et al., 2025, Molecular Cell *85*, 1838–1851
May 1, 2025 
https://doi.org/10.1016/j.molcel.2025.04.010

CellPress

CellPress

Molecular Cell

Article

# Activation of bacterial programmed cell death by phage inhibitors of host immunity

Sukrit Silas,[1,2,9,*] Héloïse Carion,[1] Kira S. Makarova,[3] Eric S. Laderman,[1] Thomas Todeschini,[4] Pradeep Kumar,[5] Matthew Johnson,[1] Michael Bocek,[6] Franklin L. Nobrega,[4] Eugene V. Koonin,[3] and Joseph Bondy-Denomy[1,7,8,*]

[1]Department of Microbiology and Immunology, University of California, San Francisco, San Francisco, CA 94158, USA
[2]Gladstone Institute of Virology, J. David Gladstone Institutes, San Francisco, CA 94158, USA
[3]National Center for Biotechnology Information, National Library of Medicine, National Institutes of Health, Bethesda, MD 20894, USA
[4]School of Biological Sciences, University of Southampton, Southampton, UK
[5]ONI Linacre house, Banbury Road, Oxford OX2 8TA, UK
[6]Twist Biosciences, South San Francisco, CA 94080, USA
[7]Innovative Genomics Institute, Berkeley, CA 94720, USA
[8]Quantitative Biosciences Institute, University of California, San Francisco, San Francisco, CA 94158, USA
[9]Lead contact
*Correspondence: sukrit.silas@gladstone.ucsf.edu (S.S.), joseph.bondy-denomy@ucsf.edu (J.B.-D.)
https://doi.org/10.1016/j.molcel.2025.04.010

## SUMMARY

Bacterial and archaeal viruses are replete with diverse uncharacterized accessory genes (AGs), which likely interface with host processes. However, large-scale discovery of virus AG functions remains challenging. Here, we developed an integrated computational and experimental discovery platform to identify viral AGs and assign functions. We show that multiple AGs activate unexpected programmed cell death (PCD) activity of distinct restriction-modification (R-M) systems. We describe an exapted type I R-M decoy that kills the host upon sensing several different anti-defense AGs and a self-guarded type III R-M system that restricts phages but also induces PCD when bound by anti-R-M proteins. Other phage counter-defense genes additionally activate non-R-M-based abortive infection systems encoded by prophages. This defense strategy creates a conundrum: lose AGs and be exposed to immunity or keep AGs and trigger PCD. Strategies employed by viruses to avoid this double bind could be an important factor in virus evolution that remains to be explored.

## INTRODUCTION

To a large extent, evolution of life is a story of the virus-host arms race.[1] As hosts evolve elaborate antiviral defense mechanisms, viruses retort with equally versatile counter-defenses, which again necessitates host adaptation. Signatures of this arms race are evident in prokaryotic genomes, where diverse defense systems tend to be encoded within "defense islands,"[2] and conversely, in virus genomes, where hotspots known as accessory regions (ARs) contain clusters of highly variable anti-defense genes (Figure 1A).[3,4] These accessory genes (AGs) are at the forefront of virus-host co-evolution: they are typically non-essential for virus reproduction, undergo frequent horizontal transfer, and diversify rapidly under enhanced evolutionary pressure.[3] Many of these genes could encode factors that target bacterial processes during phage infection. The few characterized examples of such factors perform exquisite functions, precisely creating novel interfaces in protein complexes,[5] mimicking other biomolecules to competitively inhibit defense enzymes such as restriction-modification (R-M)[6,7]; allosterically modifying cellular enzymes[8]; interfering with host functions like transcription,[9] translation,[10] CRISPR-Cas adaptive immunity,[11] motility,[12] quorum sensing,[13] and DNA transfer[14]; inhibiting other phages[15]; and even participating in inter-kingdom competition.[16] However, a vast pool of AGs in rapidly growing (meta) genomic sequence databases remains unexplored.[17] Determining the identity and functions of AGs systematically remains an important, still largely unaddressed problem.

Comparative genomic approaches can exploit the highly organized architecture of virus genomes to identify evolutionary hotspots. However, ARs have so far only been characterized in a few phage families,[3,18–22] and AGs have not been studied at a large scale. We developed a scalable, high-throughput platform to identify AGs from large datasets of phage genomes, assess their functions in a variety of bacterial strains, and identify the cognate host systems that are targeted by the AGs. Here, we deploy this platform to explore how antivirus defenses in bacteria detect and respond to phage AGs.

Recently developed systematic approaches for identification of antivirus defense systems in prokaryotes revealed an

 

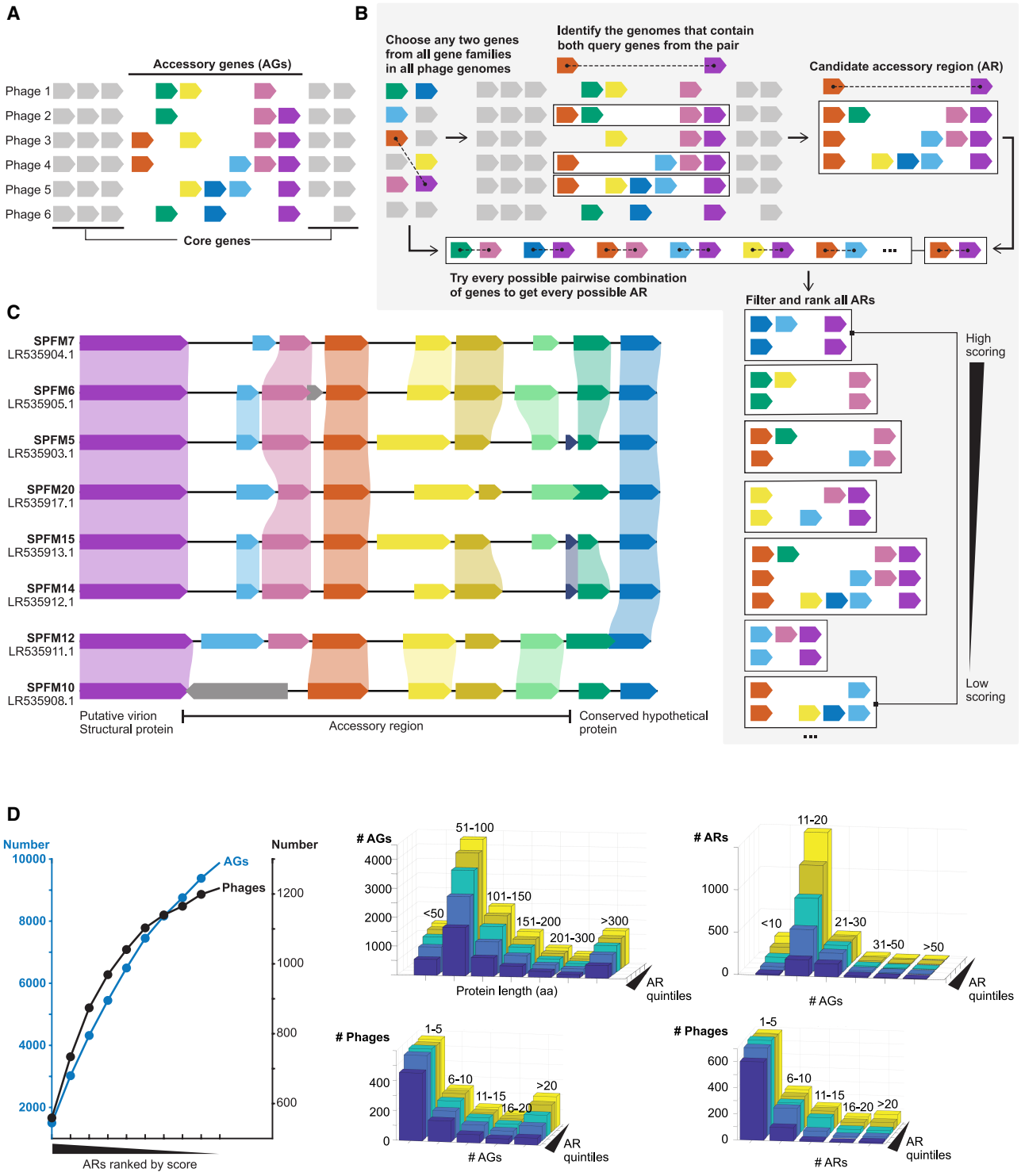


**Figure 1. Pipeline for identifying phage AGs**

(A) Schematic of a genomic region showing core (shown in gray) and accessory (in various colors) genes in a hypothetical phage genome cluster.

(B) Schematic of pipeline to exhaustively identify accessory regions (ARs) using pairwise combinations of genes, without *a priori* genome clustering. Every pairwise combination of genes is queried and candidate ARs identified in genomes containing both query genes. (Top) A hypothetical AR between orange and purple query genes. (Bottom) Several candidate ARs from other pairwise combinations of query genes. All possible ARs thus generated are filtered to remove redundancy and are ranked by complexity based on gene content, diversity, conservation, and GC content variation as a measure of horizontal transfer.

*(legend continued on next page)*

enormous, unexpected diversity of immunity mechanisms.[23–27] However, how bacteria and archaea detect viruses remains poorly understood. Recent reports present evidence that infection can be detected through recognition of phage-associated molecular patterns, that is, structural features of conserved, essential phage proteins.[28–31] We, however, identified several non-essential, counter-defense-associated phage AGs that trigger programmed cell death (PCD) responses. We propose that bacteria routinely exploit phage AGs to sense infection. Surprisingly, we find that PCD in response to counter-defense AGs is also a property of R-M systems. We describe a "self-guarded"[32] R-M system that can trigger PCD, in addition to its canonical defense functions, and another R-M locus providing "decoy" immunity.[33] Both immune strategies have previously been observed in eukaryotes, suggesting analogous themes in virus-host co-evolution across the domains of life, despite the absence of shared proteins between these convergent defense strategies in prokaryotes and eukaryotes.

## RESULTS AND DISCUSSION

### A high-throughput platform for identifying and testing phage AG functions

Given that AGs are usually defined within a cluster of closely related viruses,[18–21] AG detection is highly sensitive to the genome clustering strategy. We therefore sought to identify ARs without prior genome comparisons to define virus clusters. All genes from all phage genomes were evaluated pairwise to find all possible ARs (Figure 1B). All virus genomes that contained both genes of the pair (query pair) were initially included into a virus cluster, irrespective of genomic relatedness, and genes located between the members of the pair in all these genomes were considered potential AGs. Subsequently, a series of filters were applied. Clusters containing few viruses (<6) were removed, as ARs from these were unlikely to rank highly. Clusters comprising highly diverged viruses (<85% pairwise average nucleotide identity) were also discarded, as these could arise trivially if both query pair genes were broadly distributed. Within the surviving virus clusters, the longest ARs (>10 genes between the query pair) or those that consisted of the same genes in every genome (no AGs between the query pair, by definition) were also discarded. Subsequently, all retained ARs were scored and ranked by using a metric that evaluates gene content, diversity, conservation, and GC content variation as a measure of horizontal transfer (see STAR Methods). Our comparative genomics approach to AG identification did not rely on any functional information (for example, similarity to or location next to known counter-defense genes was not taken into account). Starting with an initial set of 1,706 Enterobacteriophage genomes, 2,014 non-redundant ARs containing 10,888 putative AGs were identified in 1,217 phages. A typical AR encompassed 11 to 30 unique AGs cumulatively across multiple related phages. A sample AR is shown in Figure 1C. Most of the AGs encoded small proteins consisting of ~50–100 amino acid (aa). A typical phage genome contained <5 ARs and <10 AGs, but some phages encoded many more AGs (Figure 1D).

We manually inspected the 200 most confidently predicted (highest-scoring) ARs and selected multiple (2–5) AGs from 62 of these for in-depth characterization (see Document S2 and Data S1 for detailed notes on each AR and rationale for AG selection). We synthesized 200 AGs, of which 54 were from ARs containing at least one known counter-defense AG (Data S1 and S2), whereas 135 AGs were from ARs consisting entirely of genes of unknown function. Eleven phage genes with previously elucidated functions were included as controls (*abc2*, *ardA*, *arn*, *cor*, *dmd*, *imm*, *ip1*, *ocr*, *ral*, *sieA*, and *stp*). Each AG was synthesized with a unique DNA barcode, enabling identification of AG functions by pooled screening. AG pools were constructed in a subset of the 72-strain *E. coli* reference (ECOR) collection[34] using Tn7 for site-specific chromosomal integration to minimize variation due to position effects (one AG per cell, and one pool per ECOR strain). AG expression was controlled with an isopropyl-b-D-thiogalactopyranoside (IPTG)-inducible promoter, and bacterial fitness was measured in triplicate by next-generation sequencing upon AG expression (Figure 2A). Proportions of cells encoding various AGs in the pools were determined using the prevalence of the corresponding AG barcodes as a proxy, and bacterial fitness was calculated by $\log_2$ transformation of the ratio of observed AG barcode count to the median count (neutral fitness) for each pool.

### Phage AGs trigger bacterial systems that cause growth inhibition

Comparing the relative barcode abundances in pre-AG and post-AG induction samples, we noticed that several AGs produced "conditional-lethal" phenotypes. These AGs imposed a severe fitness burden in only a minority of *E. coli* strains, suggesting that their expression was not generally toxic but rather induced dormancy or death through strain-specific mechanisms (Figure 2B). Abortive infection (Abi) defense systems typically kill the host cell or induce dormancy, halting phage reproduction, and many known Abi systems are activated by the production of conserved phage proteins.[28–31] We hypothesized that the strains exhibiting growth inhibition phenotypes in our screens harbor Abi-like systems that are triggered by variable phage proteins encoded by AGs. Surprisingly, some of these growth-inhibiting phage AGs were previously identified as R-M inhibitors.[35,36] Abi systems that evolved to sense anti-restriction AGs might serve as a secondary layer of immunity to thwart phage-encoded counter-defense strategies that target primary defenses like R-M.

Growth inhibition in these wild strains was triggered by some R-M inhibitors but not others, even discriminating between the

(C) A sample high-scoring AR in a family of *Salmonella* phages (name in bold, accession number below name). Shading denotes gene conservation across phage genomes.

(D) Statistical features of ARs and AGs. 2D chart depicts saturation curves (cumulative distribution functions) of unique AGs (left axis) and phage genomes (right axis), represented in ~2,000 non-redundant ARs ranked by score on the *x* axis. 3D bar graphs show various distributions (length of AGs, number of AGs per AR, number of AGs per phage, and number of ARs per phage). Color-coded histograms in each bar graph are cumulative, i.e., the first histogram (dark blue) shows the top 20% highest-scoring ARs, the next (light blue) represents top 40%, and so on.

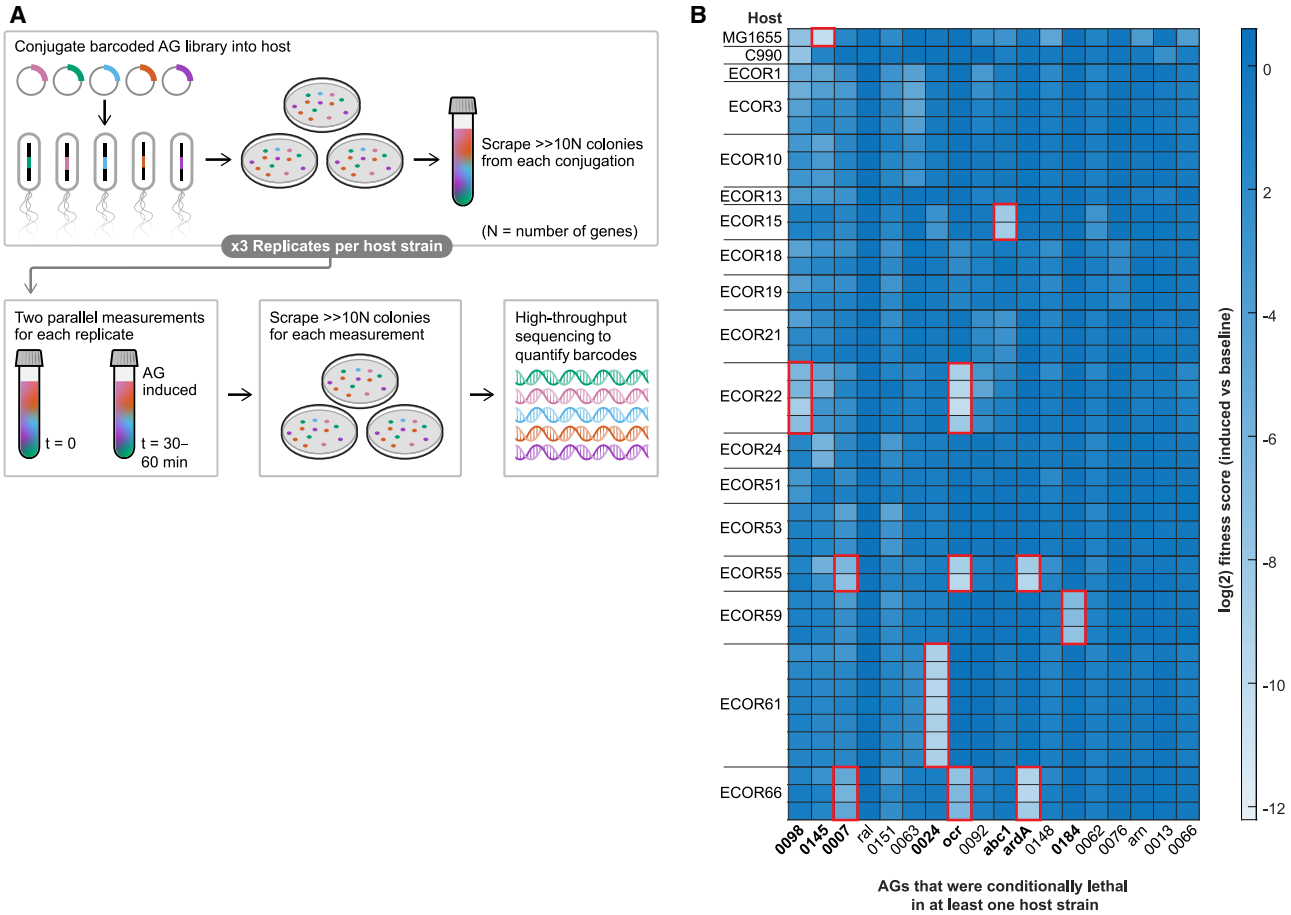


**Figure 2. High-throughput screen to test AG functions**

(A) Schematic of the AG screen. Barcoded AGs are transformed into various bacterial hosts by conjugation in triplicate. Successful transconjugant colonies (with chromosomally integrated AGs) are scraped and pooled to yield three pools per strain. In each experiment, two measurements are made for every pool, baseline (with AGs uninduced at the start) and induced (after 30–60 min of AG expression). Surviving cells are grown on agar plates (without further AG induction), and barcode representation is measured as a proxy for fitness effect of AG expression by high-throughput sequencing.

(B) Heatmap of $\log_2$-transformed fitness scores comparing induced and baseline samples. Data are averaged from three replicates of the entire screen. Additionally, most hosts were tested multiple times as part of a parallel experiment testing AG libraries with phage infection, which will be described in a separate publication. Screen results without phage infection are presented in their entirety here (thus, the 7 rows for ECOR61 mean that 7 screens were performed thrice for a total of 21 replicates). Of 200 AGs tested, only AGs that exhibited lethality in some (but not all) hosts are shown. Red boxes/bold names highlight conditional-lethal AGs selected for further study. Previously named AGs are *orf87:ral*, *orf1:ocr*, *orf116:abc1*, *orf169:ardA*, and *orf2:arn*.

two DNA mimics, Ocr[35] and ArdA[36] (Figure S1A). Notably, Ral, which operates by allosterically hyperactivating the methyltransferase (unlike Ocr and ArdA),[8] did not inhibit growth in any strains. Conversely, a previously unknown AG, *orf7* (hereafter *tro1* for trigger of Ronin 1; see decoy immunity in bacteria section below), also blocked the growth of two wild strains, ECOR55 and 66, similarly to *ocr* and *ardA*, but did not inhibit type I R-M in MG1655 (Figure S1B). Furthermore, the predicted structure of Tro1 does not resemble a DNA mimic (Data S3), and the protein is not negatively charged (pI ~4 for Ocr/ArdA, but ~8 for Tro1). These observations suggested a diversity of growth inhibition mechanisms operating in these strains, each triggered by distinct phage proteins including but not limited to DNA-mimicking R-M inhibitors.

To identify putative Abi systems activated by AGs, we chromosomally integrated various trigger AGs into the respective ECOR strains and confirmed that their expression inhibited growth (Figure 3A). We then performed genome-wide transposon suppressor screens to map the loci responsible for growth inhibition (Figure 3B). Transposon insertions in the putative Abi systems would be expected to allow growth of the bacteria despite heterologous expression of a trigger AG. By mapping transposon insertion locations in cells that survived AG induction, we identified putative Abi systems in five of the eight tested strains (Data S4). Surprisingly, all three AGs that inhibited growth of ECOR55 (*ocr*, *tro1*, and *ardA*) were apparently activating the same R-M-like system (Ronin); a distinct R-M system in ECOR22 was also triggered by *ocr*, and three prophage-associated loci were triggered by AGs with no previously ascribed functions. These systems will each be discussed in further detail below.

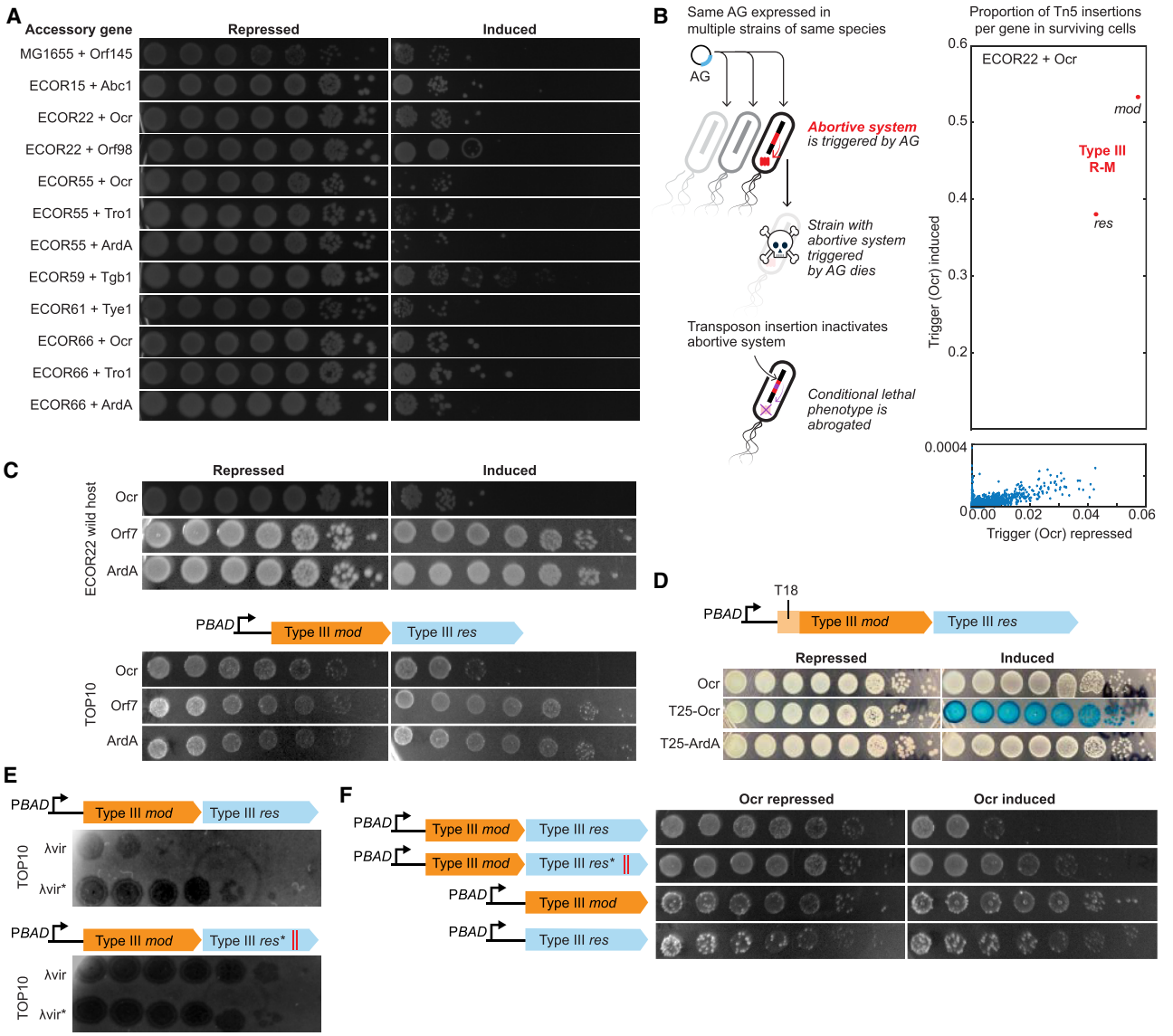


**Figure 3. AGs that trigger programmed cell death**

(A) Host-AG combinations in red boxes from Figure 2B tested individually for AG-induced lethality (serial 10-fold dilutions of saturated culture; AGs repressed: left, induced: right). AGs named in this work are *orf7:tro1*, *orf24:tye1*, and *orf184:tgb1*.

(B) Schematic depicts hypothetical strain-specific PCD system being triggered by AGs and inactivated in follow-up transposon knockout screens. Data from a representative screen with a Tn5 library constructed from ECOR22 with chromosomally encoded *ocr*. Proportion of transposon insertions per gene in surviving cells with *ocr* repressed is plotted on the *x* axis, and *ocr* induced is shown on the *y* axis. *y* axis interrupted to resolve genes other than type III R-M *mod*, *res*.

(C) Abortive phenotype of EcoR22I in its native host (top) and reconstituted (bottom) when cloned onto a plasmid and expressed in TOP10 (AGs repressed: left, induced: right). Note that top panel is reproduced from (A).

(D) Bacterial two-hybrid (BACTH) assay with adenylate cyclase (AC) fragments T25 fused to the N terminus of Ocr or ArdA and T18 fused to the N terminus of EcoR22I-Mod. Blue staining results from hydrolysis of X-gal upon reconstitution of AC fragments, which stimulates production of the β-galactosidase enzyme LacZ.

(E) Plaque assay showing R-M phenotype of EcoR22I against methylated and unmethylated λvir in TOP10. λvir* was methylated by passaging in a TOP10 strain with nuclease-dead EcoR22I (res* double mutant; D1024A, D1043A) and tested for its ability to evade restriction by wild-type or res* EcoR22I.

(F) As in (C), PCD activity of EcoR22I variants in TOP10 (wild-type, nuclease dead (res*), and *mod*, *res* genes expressed individually). pBAD indicates that the construct was overexpressed from the plasmid in (F)–(H). Representative panels from triplicate experiments shown in (A) and (C)–(F).

## A self-guarded R-M system can elicit PCD

A type III R-M system in ECOR22 (hereafter, EcoR22I) was required for growth inhibition in response to Ocr (Figure 3B), the DNA mimic that blocks both type I and type III R-M.[37] To determine whether this growth inhibition involved cell death or dormancy, we transiently expressed either Ocr or another anti-R-M DNA mimic, ArdA, in ECOR22. Transient *ocr* induction for 30 min and subsequent repression led to >1,000-fold reduction in viable cell count, and this irreversibility led us to conclude that ECOR22I induced PCD when *ocr* was expressed (Figure S2A). As expected, the induction of *ardA* had no effect.

R-M systems are ubiquitous in bacteria, and so are anti-restriction factors in phages.[38] In response, bacterial anti-anti-restriction mechanisms, such as retrons,[39] phage anti-restriction induced system (PARIS),[27] and PrrC,[7] induce PCD or dormancy as backup defense. Our results suggest that in ECOR22, the frontline (R-M) and backup (PCD) defense functions coalesced into an integrated, self-guarded defense system. To test this hypothesis directly, we reconstituted the PCD and R-M activities of EcoR22I in a model *E. coli* strain. In its native host, the *mod* and *res* genes of EcoR22I are associated with an SNF2-like helicase related to the ancillary defense island system associated with R-M (DISARM) helicase, *drmD*,[40] and all three genes are encoded in a P4 satellite prophage hotspot.[27] However, transposon insertions that suppressed Ocr toxicity in ECOR22 were found only in *mod* and *res* (Figures 3B and S3). We overexpressed the *mod* and *res* genes of EcoR22I in a lab strain of *E. coli* and found that EcoR22I caused death upon Ocr expression but not when either ArdA or Tro1 was expressed, consistent with the behavior of the wild host (Figure 3C). Ocr was not toxic in the lab strain when paired with a defective version of EcoR22I (see Figure 3D). A F54V Ocr mutant, previously reported to evade detection by PARIS,[27] also lost the ability to trigger EcoR22I-induced PCD, as did various other Ocr mutants described previously[35] (Figure S1C). Because EcoR22I is the only R-M system in the lab strain TOP10, as well as in ECOR22, EcoR22I likely detects Ocr directly, as opposed to detecting the inhibition of another R-M system. We tested this by using the bacterial two-hybrid (BACTH) assay,[41] with one fragment of the *Bordetella pertussis* adenylate cyclase fused to Ocr or ArdA and another to the N terminus of either the Mod or Res components of ECOR22I. Whereas the tagged ECOR22I constructs lost PCD activity, co-expression of tagged T25-Ocr and T18-Mod (Figure 3D) or T18-Res (Figure S4) resulted in reconstitution of the adenylate cyclase fragments *in vivo*, as indicated by an intense blue precipitate formed by β-galactosidase (β-gal) upregulation and X-gal hydrolysis. Parallel controls with expression of T25-ArdA did not yield the blue color. Thus, ECOR22I Mod and Res physically associate with Ocr (but not ArdA).

Next, we tested whether EcoR22I possesses canonical R-M activity that could block phage infection. We constructed an active site mutant of the PD-(D/E)xK restriction nuclease (res*: D1024A, D1043A double mutant) and compared immunity conferred by wild-type and res* EcoR22I against a panel of phages. EcoR22I but not the catalytic site mutant blocked λvir (Figure 3E). Furthermore, λvir passaged through the res* host (and thus modified by the EcoR22I methyltransferase) gained the ability to infect cells carrying wild-type EcoR22I, indicating that EcoR22I restricts only unmodified λvir DNA.

We then tested whether the immune (R-M) and PCD functions of EcoR22I could be uncoupled. EcoR22I *mod* and *res* individually did not induce PCD when co-expressed with *ocr*, indicating that PCD induction is a property of the complex (Figure 3F). The res* nuclease-dead mutation of EcoR22I that completely abrogated λvir restriction also decreased PCD by 100-fold (Figure 3F). These results show that the EcoR22I PD-(D/E)xK nuclease catalytic site is involved in both R-M and PCD but does not appear to be completely responsible for the latter.

Thus, EcoR22I mounts both a targeted antiviral defense and a PCD response in the presence of certain phage AG products. Coupling restriction and PCD could allow cells to respond dynamically depending on the progress of the infection.[42] This strategy parallels a self-guarded defense against herpes simplex virus type 1 (HSV-1) in human monocytes where a host protein, MORC3, has both direct antiviral activity and represses interferon production. Degradation of MORC3 by a specific HSV-1 gene product derepresses interferon, thus creating a double bind for the virus.[32]

## Decoy immunity in bacteria

A second R-M-like system also inhibited growth in the presence of anti-R-M AGs. This locus in ECOR55 encompasses *hsdS* and *hsdM* genes typical of type I R-M but lacks the nuclease (*hsdR*) and instead contains a tightly linked gene that encodes a 61-aa protein. This small gene was identified in our transposon suppressor screens as the likely toxic effector activated by Ocr, Tro1, and ArdA (Figure 4A). We named this system Ronin, after the master-less samurai in the 1962 Japanese film, *Harakiri*. We tested whether activation of Ronin caused cell death and found that transient induction of *ardA* irreversibly reduced viable colony counts of the native ECOR55 strain by $>10^4$-fold (Figure S2B). The same effect was observed in a lab strain expressing Ronin (Figure S2C). For unknown reasons, Ronin induced cell death in ECOR55 when Ocr, ArdA, or Tro1 was expressed (Figure 3A), but it no longer responded to Ocr when cloned into a lab strain (Figure 4B).

Several lines of evidence suggest that the 61-aa protein (hereafter, RonA) of Ronin is the PCD effector. The presence of a predicted transmembrane helix suggests that RonA might disrupt membrane integrity (Figure 4C). Overexpression of *ronA* alone was lethal, but this lethality was suppressed by HsdMS co-expression (Figure 4D). Removal of *ronA* inactivated Ronin, such that anti-restriction proteins no longer triggered PCD (Figure 4E). However, Ronin function was independent of the methyltransferase activity of HsdMS because PCD was not abrogated by a F287G mutation in motif IV (NPPF) of the *hsdM* catalytic domain[43] (Figure 4E). Live-cell imaging showed that Ronin activation arrested growth without lysis, which would be expected from RonA-mediated inner membrane disruption (Figure 4F). This putative mechanism is reminiscent of phage holins, which disrupt the inner membrane and allow phage endolysins to access the cell wall.[44] Endolysin-deficient phages can kill but not lyse the host.[45] To localize RonA in the cell, we constructed an mNeonGreen (mNG)-tagged version that maintained full PCD activity with its native promoter (Figure S5A) and

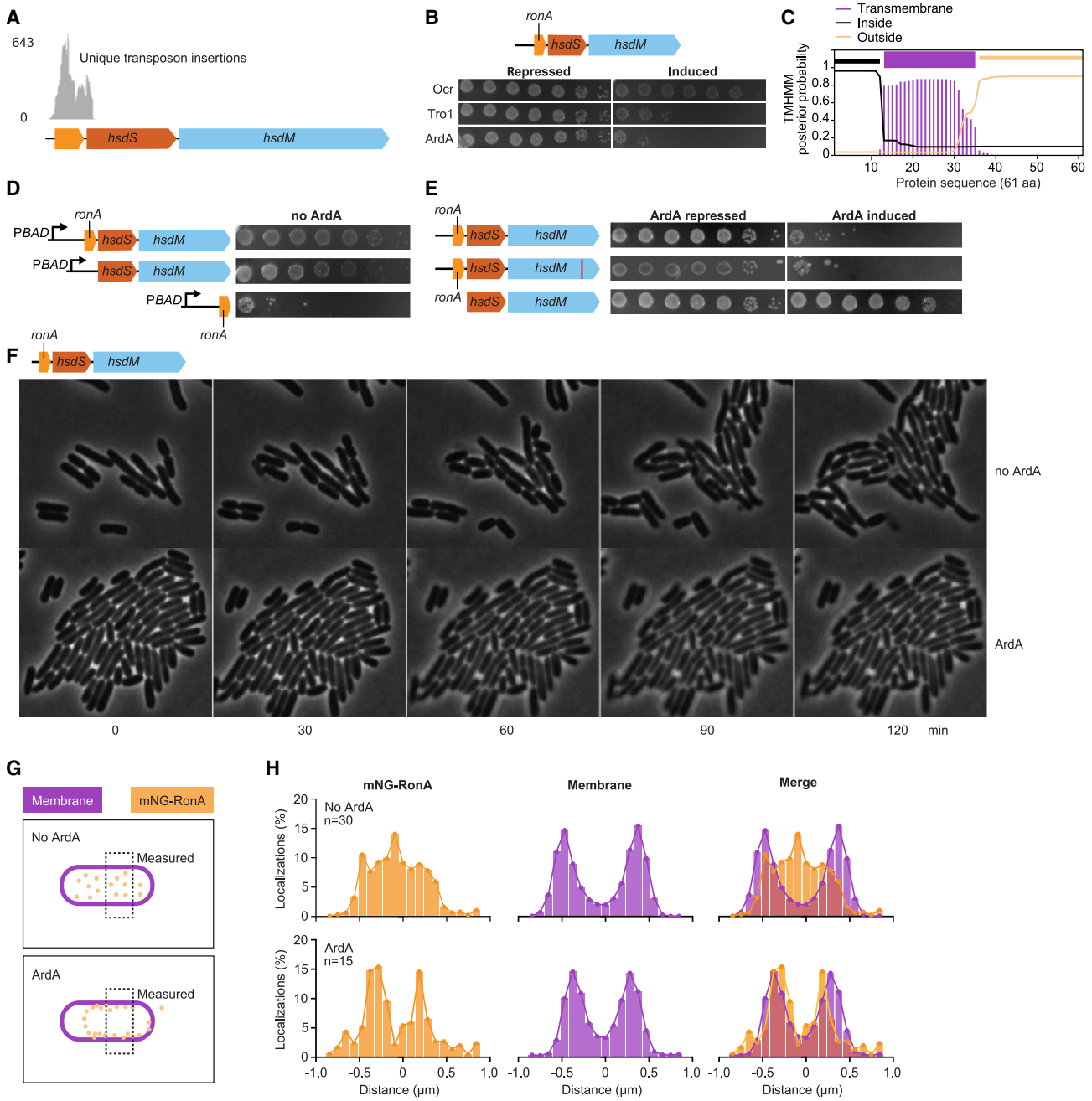


**Figure 4. A Restriction-modification-like toxin-antitoxin system**

(A) Distribution of unique transposon insertions recovered from survivors in ECOR55 Tn5 libraries upon *tro1* induction, mapped to Ronin.

(B) Schematic of Ronin system from ECOR55. Abortive phenotype reconstituted in TOP10 upon expression of Ronin from a plasmid (serial 10-fold dilutions of saturated culture; AGs repressed: left, induced: right).

(C) Prediction of transmembrane character along the 61-aa RonA sequence.

(D) Lethality of Ronin components tested when overexpressed (indicated as pBAD) without AGs.

(E) Genetic requirements for the PCD phenotype of Ronin, assayed as in (B). Red bar in *hsdM* (second row) denotes the F287G active site mutation.

(F) Time-lapse imaging of TOP10 cells expressing Ronin with (bottom) or without (top) chromosomally integrated ArdA.

(G) Schematic representation of mNeonGreen-RonA (mNG-RonA) localization by single-molecule super-resolution microscopy, with membranes shown in purple, mNG-RonA in yellow, and analyzed area as a dashed box.

(H) Localization of mNG-RonA in cells overexpressing Ronin without (top) or with (bottom) ArdA. The distribution of mNG-RonA compared with the distribution of WGA AF647 (membrane) over the cell width, 30 min post-induction of ArdA expression, is shown. Graphs represent mean distribution of 1,369 mNG-RonA localizations in ArdA-containing cells ($n = 15$) and 3,407 localizations in no-ArdA cells ($n = 30$). Representative panels from triplicate experiments shown in (B) and (D)–(F).

overexpressed mNG-RonA from an arabinose-inducible promoter. Super-resolution microscopy revealed that mNG-RonA localized to the cellular periphery upon expression of ArdA, sporadically concentrating in foci (Figure S5B), but remained dispersed throughout the cytoplasm in its absence (Figures 4G and 4H; Data S5).

As RonA was not lethal when co-expressed with HsdM and HsdS (Figure 4D), we surmise that its cell-killing activity is sequestered or suppressed by HsdMS. This model is reminiscent of PrrC activation upon inhibition of EcoPrrI restriction by T4-encoded peptide Stp. Similarly to Stp binding EcoPrrI and releasing the Abi anticodon nuclease PrrC,[7] an anti-restriction protein trigger such as ArdA could bind Ronin HsdMS to release the PCD effector, RonA. To test this model, we attempted co-immunoprecipitation (coIP) of glutathione S-transferase (GST)-tagged HsdS protein and FLAG-tagged RonA, using a dual-tagged Ronin construct, which fully retained PCD activity (Figure S5C). Without overexpression of the construct, FLAG-RonA was detected at low levels only in stationary phase cultures and did not lead to coIP with HsdS-GST (Figure S5D). Reasoning that such an association might have been disrupted during cell lysate preparation, we next employed BACTH to test binding *in vivo* and found that although HsdS physically associated with ArdA (Figure 5A), it did not interact with RonA (Figure 5B), consistent with the coIP results. The BACTH-tagged versions of Ronin retained full PCD activity (Figure 5B). Thus, although Ronin sensed ArdA directly to activate PCD, its "off" state apparently is maintained through a mechanism distinct from that in EcoPrrI-PrrC and does not involve physical sequestration of RonA by HsdMS.

We next considered that *ronA* activity might be controlled transcriptionally or translationally. These experiments were performed without overexpression of Ronin. Time-course measurements by quantitative reverse-transcription PCR (RT-qPCR) revealed that Ronin RNA was indeed elevated >10-fold across the Ronin locus within 5 min of *ardA* induction (Figure 5C). Unexpectedly, however, the levels of a 235-bp non-coding region immediately upstream of *ronA* did not change (Figure 5C). This region contributes an unknown, essential functionality because truncation of the upstream 135-bp (leaving the *ronA*-adjacent 100 bp intact) inactivated Ronin (Figure S6A), and this defect could not be rescued even by overexpressing the truncated construct (Figure S6B). We then used the dual-tagged FLAG-RonA HsdS-GST construct to measure HsdS and RonA protein levels and observed that HsdS also increased upon *ardA* induction (Figures 5C and 5D). Notably, RonA protein was undetectable prior to *ardA* induction (Figure 5D) despite almost indistinguishable *ronA* and *hsdS* RNA levels throughout the time-course experiment (Figure 5C). The switch-like production of RonA in response to *ardA* induction suggests that RonA lethality is controlled primarily at the translational level, with an additional feedback loop in which the Ronin transcript is upregulated or stabilized upon activation. Thus, Ronin appears to be a type I R-M derivative that triggers PCD when various phage AG products are detected, including anti-restriction factors such as Ocr/ArdA, as well as other proteins of unknown function such as Tro1. Therefore, multiple distinct phage AGs can activate the same bacterial defense system.

Examination of the gene neighborhoods of *ronA* homologs showed that they are always directly adjacent to *hsdS* and *hsdM* genes and occur in two predominant genetic architectures (which could be distinguished based on the presence or absence of an upstream DUF4102 integrase). Ronin is either linked to an atypical type I/type IV composite R-M system or to a bacteriophage exclusion (BREX) system (Figure 5E). The BREX-linked architecture is exclusive to *E. coli* strains, whereas the type I/IV R-M-linked architecture was found in *Salmonella*, *Klebsiella*, and *Enterobacter*. Most (77%) Ronin-encoding *E. coli* genomes lack *hsdR* genes (Data S6), so recruitment of a *trans*-acting HsdR to fulfill a canonical immune function is not possible. The nuclease-less configuration of the systems in *E. coli* suggests that PCD is the primary function of Ronin. This functionality is reminiscent of decoy immunity (especially common in plants), where a host defense factor mimics the target of a pathogen effector. The effector then binds the decoy instead of its actual target, such as associated R-M or BREX systems, and the decoy alerts the host to the presence of the pathogen resulting in PCD induction.[33]

Although Ronin lost the *hsdR* defense nuclease, it still encodes the native target of Ocr/ArdA, i.e., the type I R-M HsdMS complex, and its activation depends on Ocr/ArdA binding HsdMS. Consistent with this, Ronin could still sense the Ocr F54V mutant that retains anti-restriction activity but evades recognition by PARIS[27] and EcoR22I (Figure S1C). Surprisingly, however, Ronin also responded to various Ocr mutants that lost their anti-restriction activity (Figure S1C). Because it is almost always linked to an R-M or BREX system, both of which can be blocked by Ocr,[46] Ronin might drive evolution of Ocr-encoding phages to a BREX/R-M susceptible state through the loss of Ocr. Decoy immunity could thus be a powerful host strategy to constrain virus escape from bacterial restriction systems.

## Counter-defense-associated AGs trigger Abi mechanisms encoded in prophages

We identified three prophage-encoded Abi loci that inhibited bacterial growth in response to counter-defense-associated AGs (Data S4). First, we found that heterologous expression of *orf116*, the poorly characterized *abc1* gene of phage P22 that is adjacent to the RecBCD inhibitor *abc2* (Figure 6A),[47] inhibited the growth of ECOR15. Transposon insertions identified the P4 satellite prophage (in particular, the ~100-bp intergenic region marked by a star in Figure 6A, which contains the P4 late promoters[48]) as the Abi locus (Figure S3). We cloned the entire prophage into a plasmid and reconstituted the growth inhibition phenotype in a lab strain. The "defense hotspot"[27] of this particular P4 variant was empty, indicating that in this case the prophage itself was responsible for the Abi phenotype. However, P4 cannot enter the lytic cycle without a co-resident P2 prophage (which was absent in the lab strain), apparently ruling out prophage induction as the mechanism of growth inhibition. Thus, it remains unclear how *orf116* triggers P4 toxicity.

Second, the gop-beta-cII Abi system is a toxin-antitoxin-like module located in a P4 defense hotspot with previously demonstrated anti-phage activity,[27,49] but its trigger had not been identified so far. Our suppressor screen data (Figure S3) showed that

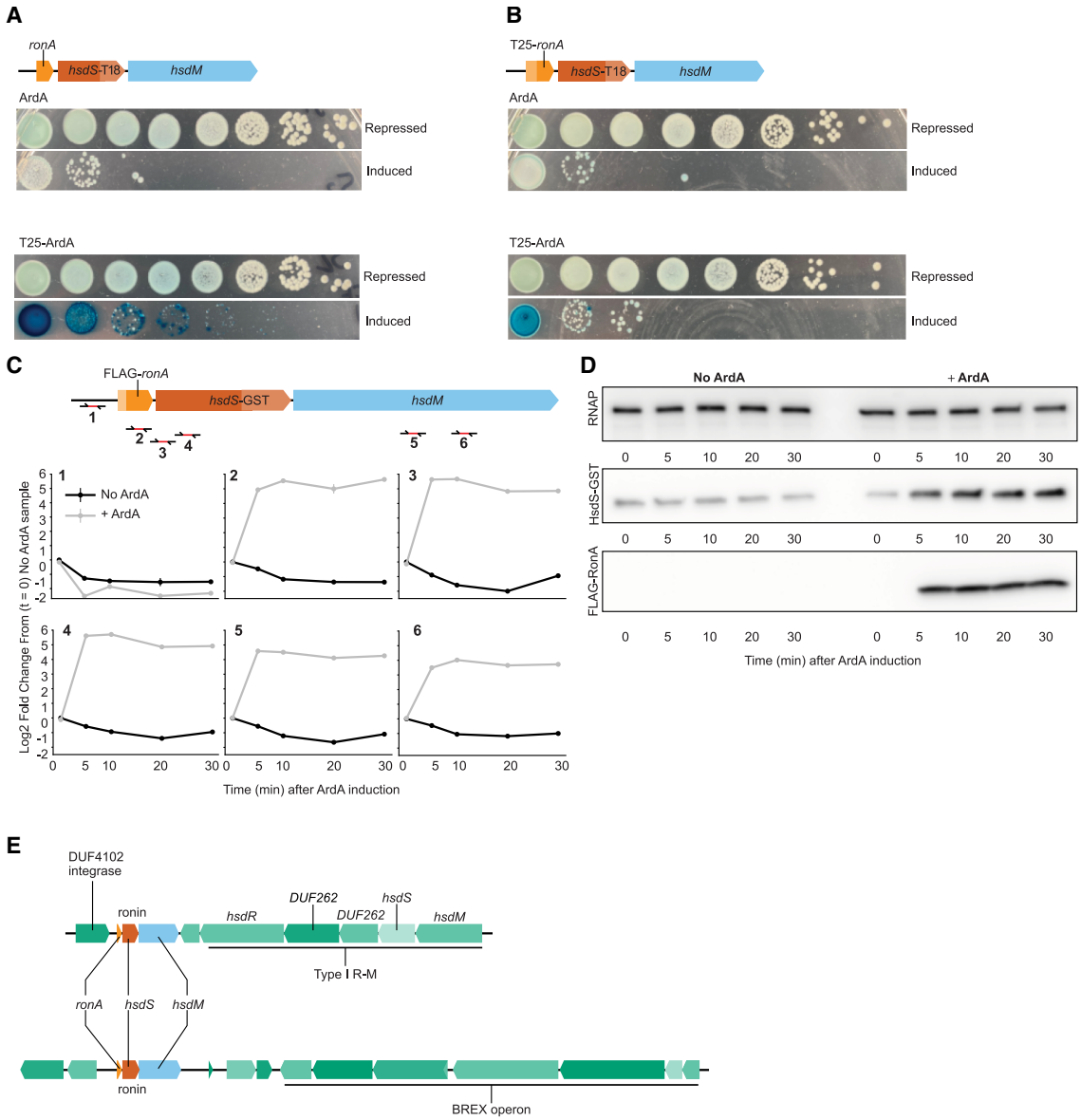


**Figure 5. Decoy immunity in bacteria**

(A) BACTH assay with T18 fused to the C terminus of Ronin HsdS, and ArdA supplied with or without an N-terminal T25 tag. PCD activation measured upon ArdA expression by plating serial 10-fold dilutions of saturated culture. Blue staining indicates reconstitution of T18 and T25 fragments.

(B) As in (A), but with an additional N-terminal T25 tag on RonA.

(C) Time-course measurements (average of three replicates) of Ronin transcription levels by quantitative reverse-transcription PCR (RT-qPCR) from parallel log-phase cultures of cells engineered with and without *ardA*, each carrying plasmid-encoded dual-tagged FLAG-RonA HsdS-GST Ronin. Locations of qPCR amplicons are depicted along the operon and correspond to numbered graphs that show transcription dynamics before (t = 0) and after (t = 5, 10, 20, 30 min) IPTG addition to cultures to induce *ardA*. In each graph, fold changes at each time point for both ±ArdA cultures were calculated relative to the amplicon level at t = 0 in the no-ArdA sample.

(D) Western blotting to measure HsdS-GST and FLAG-RonA protein levels in whole-cell lysates prepared from the same time-course cultures as in (C). *E. coli* RNAP is included as a loading control.

(E) Two prevalent architectures of *ronA*-linked type I R-M-like PCD system (Ronin), distinguished by the presence of an upstream DUF4102 integrase. Representative panels from triplicate experiments shown in (A) and (B).

gop-beta-cII toxicity is activated by *orf184* (hereafter, *tgb1* for trigger of gop-beta-cII), which is present in the same AR as the anti-restriction gene *ral* in a group of Enterobacteriophages (Figure 6B). We cloned gop-beta-cII into a lab strain and confirmed that expressing *tgb1* caused growth inhibition in a gop-beta-cII-dependent manner (Figure 6B).

Finally, a distinct prophage-encoded system in ECOR61 inhibited growth upon expression of *orf24* (hereafter, *tye1* for trigger

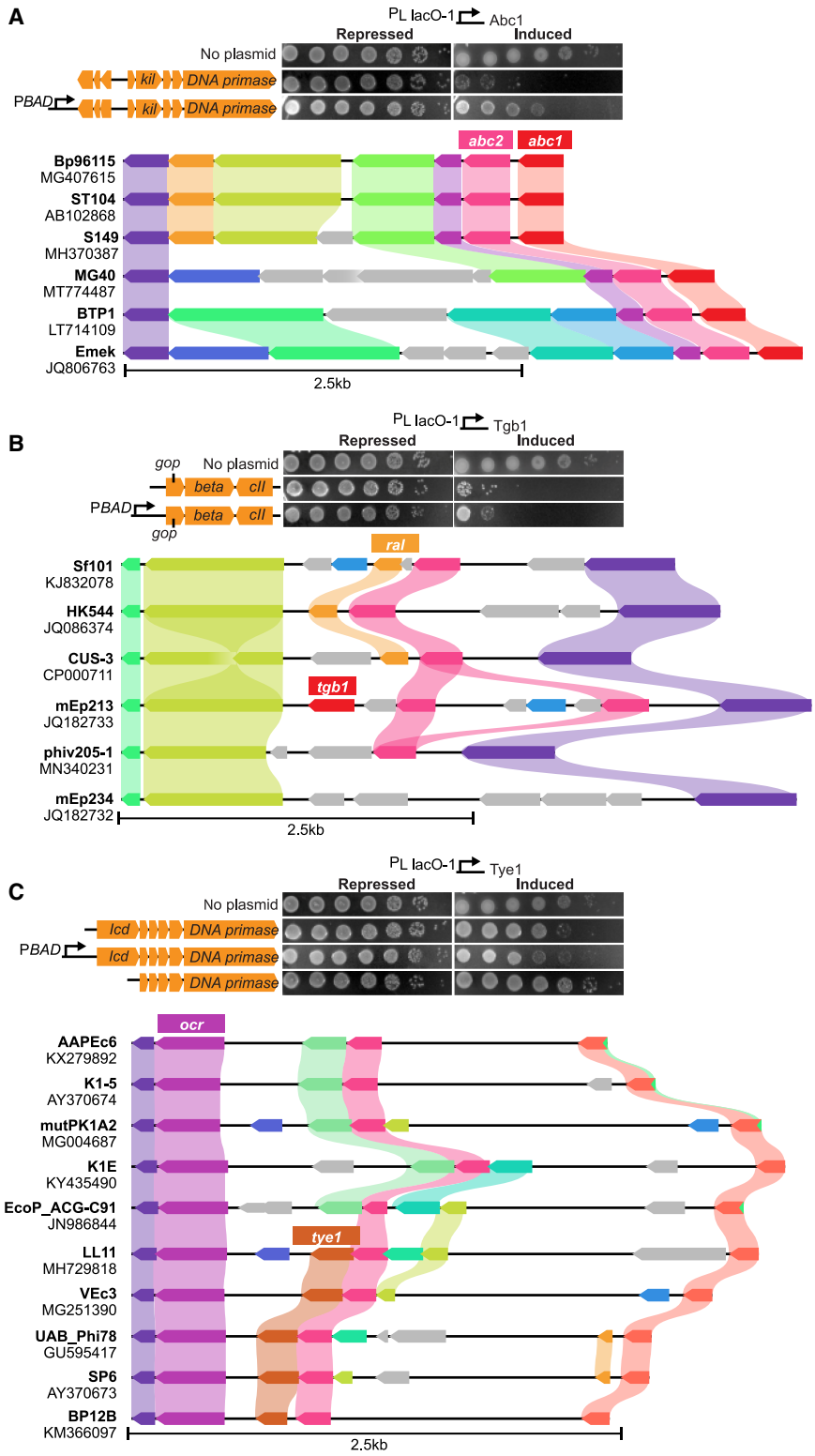


**Figure 6. AGs that trigger prophage-encoded PCD mechanisms**

(A) Abortive phenotype of P4 satellite prophage from ECOR15 cloned onto a plasmid and expressed in TOP10. *abc1* is expressed from a single-copy chromosomal insertion (serial 10-fold dilutions of saturated culture; AGs repressed: left, induced: right). Star marks an intergenic region containing P4 late-cycle promoters, which was strongly targeted in transposon suppressor screens.

(B) As in (A), PCD phenotype of gop-beta-cII system from ECOR59 upon expression of *tgb1*.

(C) As in (A), PCD phenotype of prophage-encoded superinfection exclusion system from ECOR61 upon expression of *tye1*. pBAD indicates where the constructs were overexpressed in (A)–(C). Accessory regions where trigger AGs (*abc1*, *tgb1*, *tye1*) in (A)–(C) were found with co-occurring counter-defense AGs (anti-RecBCD *abc2*, anti-R-M *ocr*, anti-R-M *ral*) are shown in the respective panels. Each row is a phage genome with name (bold) and accession indicated. Representative panels from triplicate experiments are shown.

of Yemaya), which is present in the same AR with the anti-restriction gene *ocr* in certain Enterobacteriophages (Figure 6C). We named this system "Yemaya" after the Yoruba goddess of creation and protection. Although transposon insertions that suppressed the toxicity elicited by *tye1* expression were found in three upstream Yemaya genes (Figure S3), expression of all six genes (including a DNA primase and an Icd-like cell division inhibitor with a long N-terminal extension [superfamily cl41269]) was necessary to recapitulate the Abi phenotype in a lab strain, albeit still yielding a muted effect (Figure 6C) compared with the native host (Figure 3A). The Icd-like protein is the likely effector in Yemaya as growth inhibition was abrogated upon its removal (Figure 6C).

All three prophage-encoded Abi constructs can be safely overexpressed in the lab strain, confirming that their growth inhibition activity is specifically elicited by the respective trigger AGs (Figures 6A–6C). These findings demonstrate that prophages can activate diverse Abi mechanisms in response to highly variable phage AGs.

## Conclusion

We conducted a high-throughput survey of phage AGs to probe bacterial antivirus immunity and unexpectedly discovered exaptation of R-M systems that are triggered by anti-restriction proteins to induce PCD. Our results further expand the conceptual framework of layered anti-phage defense in bacteria, whereby anti-anti-restriction mechanisms, such as retrons,[39] PARIS,[27] PrrC,[7] and CRISPR-Cas-associated toxin-antitoxin systems[50] provide backup immunity via Abi. Apparently, inactivation of cellular antiviral defenses can be used by bacteria as a signal to determine when infection has progressed too far for immunity to be efficient such that PCD becomes the defense strategy of choice.[42] In particular, we showed that EcoR22I combines both R-M and PCD functions, and Ronin is a PCD mechanism that mimics an R-M system to thwart anti-R-M AGs. These systems showcase the self-guarded and decoy immunity strategies, respectively. Both these strategies have been previously observed in eukaryotes,[32,33] demonstrating functional analogy between antiviral defense strategies in prokaryotes and eukaryotes, although the immune systems involved are not homologous. Our approach highlights how experimental assays for AGs in wild bacterial strains can uncover defense functions that cannot be identified by comparison with known defense or counter-defense factors. For instance, EcoR22I does not contain any domains currently known to be involved in PCD. Similarly, *ronA* toxins have no previously characterized links to R-M. These observations underscore and extend the concept that integration of immunity and PCD is a general feature of antiviral defense in prokaryotes.[42,51]

Assaying AGs individually in diverse hosts directly identifies otherwise elusive triggers of defense systems. Anti-phage defense systems, in particular those inducing PCD, have been shown to sense highly conserved structural features of phages (nucleic acids, capsids, terminases, or portal proteins).[28–31] We show here that a variety of poorly conserved phage AGs can also trigger defense mechanisms in the host and its prophages. In particular, the same defense system can sense disparate, unrelated AGs. Non-essential gene products might seem ill-suited for this role because the virus could simply lose the gene to escape detection. However, all AGs we found to trigger PCD are associated with common counter-defense functions, such as R-M inhibition, trapping the virus into a Scylla vs. Charybdis catch where a counter-defense AG triggers PCD upon infection, whereas losing that AG renders the virus vulnerable to immunity. The strategies viruses might have evolved to navigate this treacherous narrows are currently unknown and might be an important force in virus evolution. The host counterpoints to virus AGs were likely overlooked because many viruses encoding inhibitors and triggers of specialized host defenses can be difficult to procure and culture. Advanced technologies for DNA synthesis and high-throughput experimental platforms of the type developed in this work, combined with rapidly growing metagenomic sequence databases, are expected to yield a more complete picture of virus-host co-evolution.

## Limitations of the study

There are many more phage AGs than could be investigated in the present study. Methods to improve throughput of our functional screening assays remain an active area of investigation. This would allow us to avoid the time-consuming step of manually inspecting phage ARs to choose the most promising AG candidates. Additionally, screening AG phenotypes by a methodology that generates richly textured data (for instance, massively multiplexed single-cell RNA sequencing with barcode capture to deconvolve pooled libraries) might reveal subtle effects of AG expression on bacterial physiology that could be missed by fitness-based screening. Next, transposon insertion sequencing to identify PCD mechanisms in bacterial genomes is a powerful technique, but it cannot deconvolve instances where multiple PCD systems co-ordinate a response to the same AG. Finally, while the PCD systems are identified in wild bacterial strains where they are natively regulated, it can be very difficult to test their functions in the context of phage infection in these strains because most model coliphages are blocked by wild *E. coli*. Moreover, as our experiments with bacterial immunity are performed only in standardized high-growth conditions, we might not be able to decipher nuanced lifestyles (such as bacterial tolerance of persistent phage infection) when bacteria are not rapidly dividing.

## RESOURCE AVAILABILITY

### Lead contact

Requests for further information and resources should be directed to and will be fulfilled by the lead contact, Sukrit Silas (Sukrit.silas@gladstone.ucsf.edu).

### Materials availability

All unique/stable reagents generated in this study are available from the lead contact with a completed materials transfer agreement.

### Data and code availability

- High-throughput sequencing data have been deposited at SRA with accession PRJNA952709 and are publicly available as of the date of publication.
- Original microscopy data have been deposited at Mendeley at https://doi.org/10.17632/b722nfy9hv.1 and are publicly available as of the date of publication.

- All original code is publicly available on GitHub at https://github.com/sukritsilas/phagent.
- Any additional information required to reanalyze the data reported in this paper is available from the lead contact upon request.

## ACKNOWLEDGMENTS

S.S. was supported by the Damon Runyon Fellowship award (DRG 2352-19). Experiments were funded by awards to J.B.-D. by the Vallee, Searle, and Kleberg Foundations and NIH (R01 AI167412). K.S.M. and E.V.K. are supported by intramural funds of the US Department of Health and Human Services (National Institutes of Health, National Library of Medicine). We thank Jason Peters for technical discussions; Andy Millard for the Enterobacteriophage genome dataset; Tami Tolpa for graphic design; and Ry Young, Andrew Fire, Carol Gross, and Jonathan Weissman for guidance.

## AUTHOR CONTRIBUTIONS

Conceptualization, S.S. and J.B.-D.; methodology, S.S. and E.S.L.; software, S.S.; investigation, S.S., H.C., T.T., and P.K.; formal analysis, S.S., H.C., M.J., K.S.M., and E.V.K.; visualization, S.S., H.C., M.J., K.S.M., and T.T.; writing – original draft, S.S. and H.C.; writing – reviewing and editing, S.S., H.C., M. B., T.T., P.K., F.L.N., E.V.K., and J.B.-D.; supervision, S.S. and J.B.-D.; funding acquisition, J.B.-D.

## DECLARATION OF INTERESTS

S.S. is a co-founder and equity holder in BillionToOne, Inc. and a scientific advisory board member for Junevity, Inc. P.K. is a full-time employee of ONI. M.B. is a full-time employee of Twist. J.B.-D. is a scientific advisory board member of SNIPR Biome, Excision Biotherapeutics, and LeapFrog Bio; consults for BiomX; and is a scientific advisory board member and co-founder of Acrigen Biosciences. The Bondy-Denomy lab received research support from Felix Biotechnology.

## STAR★METHODS

Detailed methods are provided in the online version of this paper and include the following:

- KEY RESOURCES TABLE
- EXPERIMENTAL MODEL AND STUDY PARTICIPANT DETAILS
- METHOD DETAILS
  - AG conjugation into host strains
  - DNA extraction and Nextera whole-genome sequencing
  - Phage propagation and plaque assays
  - AG library preparation and NGS verification for testing post-conjugation evenness
  - AG screen
  - RB-TnSeq Tn5 library construction
  - Tn5 suppressor screen to find abortive loci
  - Verification of abortive loci activity
  - Verification of PCD by abortive systems
  - Co-immunoprecipitation of RonA and HsdS
  - Bacterial two-hybrid assay
  - Live-cell and super-resolution microscopy
  - Timecourse measurements of Ronin transcription and translation
- QUANTIFICATION AND STATISTICAL ANALYSIS
  - Computational pipeline to identify phage accessory regions
  - Runtime performance
  - AG screen data analysis
  - RB-TnSeq data analysis
  - Tn5 suppressor screen data analysis
  - Comparative analysis of Ronin systems

## SUPPLEMENTAL INFORMATION

Supplemental information can be found online at https://doi.org/10.1016/j.molcel.2025.04.010.

Received: August 23, 2023
Revised: March 4, 2025
Accepted: April 7, 2025
Published: May 1, 2025

## REFERENCES

1. Koonin, E.V., and Wolf, Y.I. (2012). Evolution of microbes and viruses: a paradigm shift in evolutionary biology? Front. Cell. Infect. Microbiol. *2*, 119. https://doi.org/10.3389/fcimb.2012.00119.
2. Koonin, E.V., Makarova, K.S., and Wolf, Y.I. (2017). Evolutionary Genomics of Defense Systems in Archaea and Bacteria. Annu. Rev. Microbiol. *71*, 233–261. https://doi.org/10.1146/annurev-micro-090816-093830.
3. Cumby, N., Davidson, A.R., and Maxwell, K.L. (2012). The moron comes of age. Bacteriophage *2*, 225–228. https://doi.org/10.4161/bact.23146.
4. Roucourt, B., and Lavigne, R. (2009). The role of interactions between phage and bacterial proteins within the infected cell: a diverse and puzzling interactome. Environ. Microbiol. *11*, 2789–2805. https://doi.org/10.1111/j.1462-2920.2009.02029.x.
5. Bingham, R., Ekunwe, S.I., Falk, S., Snyder, L., and Kleanthous, C. (2000). The major head protein of bacteriophage T4 binds specifically to elongation factor Tu. J. Biol. Chem. *275*, 23219–23226. https://doi.org/10.1074/jbc.M002546200.
6. Krüger, D.H., Schroeder, C., Hansen, S., and Rosenthal, H.A. (1977). Active protection by bacteriophages T3 and T7 against E. coli B- and K-specific restriction of their DNA. Mol. Gen. Genet. *153*, 99–106. https://doi.org/10.1007/BF01036001.
7. Penner, M., Morad, I., Snyder, L., and Kaufmann, G. (1995). Phage T4-coded Stp: double-edged effector of coupled DNA and tRNA-restriction systems. J. Mol. Biol. *249*, 857–868. https://doi.org/10.1006/jmbi.1995.0343.
8. Loenen, W.A., and Murray, N.E. (1986). Modification enhancement by the restriction alleviation protein (Ral) of bacteriophage lambda. J. Mol. Biol. *190*, 11–22. https://doi.org/10.1016/0022-2836(86)90071-9.
9. Osuna, B.A., Karambelkar, S., Mahendra, C., Sarbach, A., Johnson, M.C., Kilcher, S., and Bondy-Denomy, J. (2020). Critical Anti-CRISPR Locus Repression by a Bi-functional Cas9 Inhibitor. Cell Host Microbe *28*, 23–30.e5. https://doi.org/10.1016/j.chom.2020.04.002.
10. Mizuno, C.M., Guyomar, C., Roux, S., Lavigne, R., Rodriguez-Valera, F., Sullivan, M.B., Gillet, R., Forterre, P., and Krupovic, M. (2019). Numerous cultivated and uncultivated viruses encode ribosomal proteins. Nat. Commun. *10*, 752. https://doi.org/10.1038/s41467-019-08672-6.
11. Bondy-Denomy, J., Pawluk, A., Maxwell, K.L., and Davidson, A.R. (2013). Bacteriophage genes that inactivate the CRISPR/Cas bacterial immune system. Nature *493*, 429–432. https://doi.org/10.1038/nature11723.
12. Chung, I.Y., Jang, H.J., Bae, H.W., and Cho, Y.H. (2014). A phage protein that inhibits the bacterial ATPase required for type IV pilus assembly. Proc. Natl. Acad. Sci. USA *111*, 11503–11508. https://doi.org/10.1073/pnas.1403537111.
13. Shah, M., Taylor, V.L., Bona, D., Tsao, Y., Stanley, S.Y., Pimentel-Elardo, S.M., McCallum, M., Bondy-Denomy, J., Howell, P.L., Nodwell, J.R., et al. (2021). A phage-encoded anti-activator inhibits quorum sensing in Pseudomonas aeruginosa. Mol. Cell *81*, 571–583.e6. https://doi.org/10.1016/j.molcel.2020.12.011.
14. Lu, M.J., and Henning, U. (1994). Superinfection exclusion by T-even-type coliphages. Trends Microbiol. *2*, 137–139. https://doi.org/10.1016/0966-842x(94)90601-7.

15. Li, B.H., Kwasniewski, M., Kirchner, J., and Bockrath, R. (1992). RexAB proteins of bacteriophage lambda enhance the effect of photolyase-dimer complexes on lacZ gene expression in Escherichia coli. Mol. Gen. Genet. *231*, 480–484. https://doi.org/10.1007/BF00292719.

16. Brüssow, H., Canchaya, C., and Hardt, W.D. (2004). Phages and the evolution of bacterial pathogens: from genomic rearrangements to lysogenic conversion. Microbiol. Mol. Biol. Rev. *68*, 560–602. https://doi.org/10.1128/MMBR.68.3.560-602.2004.

17. Kristensen, D.M., Mushegian, A.R., Dolja, V.V., and Koonin, E.V. (2010). New dimensions of the virus world discovered through metagenomics. Trends Microbiol. *18*, 11–19. https://doi.org/10.1016/j.tim.2009.11.003.

18. Juhala, R.J., Ford, M.E., Duda, R.L., Youlton, A., Hatfull, G.F., and Hendrix, R.W. (2000). Genomic sequences of bacteriophages HK97 and HK022: pervasive genetic mosaicism in the lambdoid bacteriophages. J. Mol. Biol. *299*, 27–51. https://doi.org/10.1006/jmbi.2000.3729.

19. Comeau, A.M., Bertrand, C., Letarov, A., Tétart, F., and Krisch, H.M. (2007). Modular architecture of the T4 phage superfamily: a conserved core genome and a plastic periphery. Virology *362*, 384–396. https://doi.org/10.1016/j.virol.2006.12.031.

20. Bondy-Denomy, J., Qian, J., Westra, E.R., Buckling, A., Guttman, D.S., Davidson, A.R., and Maxwell, K.L. (2016). Prophages mediate defense against phage infection through diverse mechanisms. ISME J. *10*, 2854–2866. https://doi.org/10.1038/ismej.2016.79.

21. Tsao, Y.F., Taylor, V.L., Kala, S., Bondy-Denomy, J., Khan, A.N., Bona, D., Cattoir, V., Lory, S., Davidson, A.R., and Maxwell, K.L. (2018). Phage Morons Play an Important Role in Pseudomonas aeruginosa Phenotypes. J. Bacteriol. *200*, e00189-18. https://doi.org/10.1128/JB.00189-18.

22. Repoila, F., Tétart, F., Bouet, J.Y., and Krisch, H.M. (1994). Genomic polymorphism in the T-even bacteriophages. EMBO J. *13*, 4181–4192. https://doi.org/10.1002/j.1460-2075.1994.tb06736.x.

23. Doron, S., Melamed, S., Ofir, G., Leavitt, A., Lopatina, A., Keren, M., Amitai, G., and Sorek, R. (2018). Systematic discovery of antiphage defense systems in the microbial pangenome. Science *359*, eaar4120. https://doi.org/10.1126/science.aar4120.

24. Gao, L., Altae-Tran, H., Böhning, F., Makarova, K.S., Segel, M., Schmid-Burgk, J.L., Koob, J., Wolf, Y.I., Koonin, E.V., and Zhang, F. (2020). Diverse enzymatic activities mediate antiviral immunity in prokaryotes. Science *369*, 1077–1084. https://doi.org/10.1126/science.aba0372.

25. Millman, A., Melamed, S., Leavitt, A., Doron, S., Bernheim, A., Hör, J., Garb, J., Bechon, N., Brandis, A., Lopatina, A., et al. (2022). An expanded arsenal of immune systems that protect bacteria from phages. Cell Host Microbe *30*, 1556–1569.e5. https://doi.org/10.1016/j.chom.2022.09.017.

26. Vassallo, C.N., Doering, C.R., Littlehale, M.L., Teodoro, G.I.C., and Laub, M.T. (2022). A functional selection reveals previously undetected anti-phage defence systems in the E. coli pangenome. Nat. Microbiol. *7*, 1568–1579. https://doi.org/10.1038/s41564-022-01219-4.

27. Rousset, F., Depardieu, F., Miele, S., Dowding, J., Laval, A.L., Lieberman, E., Garry, D., Rocha, E.P.C., Bernheim, A., and Bikard, D. (2022). Phages and their satellites encode hotspots of antiviral systems. Cell Host Microbe *30*, 740–753.e5. https://doi.org/10.1016/j.chom.2022.02.018.

28. Lopatina, A., Tal, N., and Sorek, R. (2020). Abortive Infection: Bacterial Suicide as an Antiviral Immune Strategy. Annu. Rev. Virol. *7*, 371–384. https://doi.org/10.1146/annurev-virology-011620-040628.

29. Gao, L.A., Wilkinson, M.E., Strecker, J., Makarova, K.S., Macrae, R.K., Koonin, E.V., and Zhang, F. (2022). Prokaryotic innate immunity through pattern recognition of conserved viral proteins. Science *377*, eabm4096. https://doi.org/10.1126/science.abm4096.

30. Zhang, T., Tamman, H., Coppieters 't Wallant, K., Kurata, T., LeRoux, M., Srikant, S., Brodiazhenko, T., Cepauskas, A., Talavera, A., Martens, C., et al. (2022). Direct activation of a bacterial innate immune system by a viral capsid protein. Nature *612*, 132–140. https://doi.org/10.1038/s41586-022-05444-z.

31. Stokar-Avihail, A., Fedorenko, T., Hör, J., Garb, J., Leavitt, A., Millman, A., Shulman, G., Wojtania, N., Melamed, S., Amitai, G., and Sorek, R. (2023). Discovery of phage determinants that confer sensitivity to bacterial immune systems. Cell *186*, 1863–1876.e16. https://doi.org/10.1016/j.cell.2023.02.029.

32. Gaidt, M.M., Morrow, A., Fairgrieve, M.R., Karr, J.P., Yosef, N., and Vance, R.E. (2021). Self-guarding of MORC3 enables virulence factor-triggered immunity. Nature *600*, 138–142. https://doi.org/10.1038/s41586-021-04054-5.

33. Moffett, P. (2016). Using Decoys to Detect Pathogens: An Integrated Approach. Trends Plant Sci. *21*, 369–370. https://doi.org/10.1016/j.tplants.2016.04.002.

34. Ochman, H., and Selander, R.K. (1984). Standard reference strains of Escherichia coli from natural populations. J. Bacteriol. *157*, 690–693. https://doi.org/10.1128/JB.157.2.690-693.1984.

35. Roberts, G.A., Stephanou, A.S., Kanwar, N., Dawson, A., Cooper, L.P., Chen, K., Nutley, M., Cooper, A., Blakely, G.W., and Dryden, D.T.F. (2012). Exploring the DNA mimicry of the Ocr protein of phage T7. Nucleic Acids Res. *40*, 8129–8143. https://doi.org/10.1093/nar/gks516.

36. McMahon, S.A., Roberts, G.A., Johnson, K.A., Cooper, L.P., Liu, H., White, J.H., Carter, L.G., Sanghvi, B., Oke, M., Walkinshaw, M.D., et al. (2009). Extensive DNA mimicry by the ArdA anti-restriction protein and its role in the spread of antibiotic resistance. Nucleic Acids Res. *37*, 4887–4897. https://doi.org/10.1093/nar/gkp478.

37. Krüger, D.H., Reuter, M., Hansen, S., and Schroeder, C. (1982). Influence of phage T3 and T7 gene functions on a type III(EcoP1) DNA restriction-modification system in vivo. Mol. Gen. Genet. *185*, 457–461. https://doi.org/10.1007/BF00334140.

38. Vasu, K., and Nagaraja, V. (2013). Diverse functions of restriction-modification systems in addition to cellular defense. Microbiol. Mol. Biol. Rev. *77*, 53–72. https://doi.org/10.1128/MMBR.00044-12.

39. Millman, A., Bernheim, A., Stokar-Avihail, A., Fedorenko, T., Voichek, M., Leavitt, A., Oppenheimer-Shaanan, Y., and Sorek, R. (2020). Bacterial Retrons Function In Anti-Phage Defense. Cell *183*, 1551–1561.e12. https://doi.org/10.1016/j.cell.2020.09.065.

40. Ofir, G., Melamed, S., Sberro, H., Mukamel, Z., Silverman, S., Yaakov, G., Doron, S., and Sorek, R. (2018). DISARM is a widespread bacterial defence system with broad anti-phage activities. Nat. Microbiol. *3*, 90–98. https://doi.org/10.1038/s41564-017-0051-0.

41. Karimova, G., Pidoux, J., Ullmann, A., and Ladant, D. (1998). A bacterial two-hybrid system based on a reconstituted signal transduction pathway. Proc. Natl. Acad. Sci. USA *95*, 5752–5756. https://doi.org/10.1073/pnas.95.10.5752.

42. Koonin, E.V., and Zhang, F. (2017). Coupling immunity and programmed cell suicide in prokaryotes: Life-or-death choices. BioEssays *39*, 1–9. https://doi.org/10.1002/bies.201600186.

43. Murray, N.E. (2000). Type I restriction systems: sophisticated molecular machines (a legacy of Bertani and Weigle). Microbiol. Mol. Biol. Rev. *64*, 412–434. https://doi.org/10.1128/MMBR.64.2.412-434.2000.

44. Young, R. (1992). Bacteriophage lysis: mechanism and regulation. Microbiol. Rev. *56*, 430–481. https://doi.org/10.1128/mr.56.3.430-481.1992.

45. Paul, V.D., Sundarrajan, S., Rajagopalan, S.S., Hariharan, S., Kempashanaiah, N., Padmanabhan, S., Sriram, B., and Ramachandran, J. (2011). Lysis-deficient phages as novel therapeutic agents for controlling bacterial infection. BMC Microbiol. *11*, 195. https://doi.org/10.1186/1471-2180-11-195.

46. Isaev, A., Drobiazko, A., Sierro, N., Gordeeva, J., Yosef, I., Qimron, U., Ivanov, N.V., and Severinov, K. (2020). Phage T7 DNA mimic protein Ocr is a potent inhibitor of BREX defence. Nucleic Acids Res. *48*, 5397–5406. https://doi.org/10.1093/nar/gkaa290.

47. Murphy, K.C. (2000). Bacteriophage P22 Abc2 protein binds to RecC increases the 5′ strand nicking activity of RecBCD and together with lambda

bet, promotes Chi-independent recombination. J. Mol. Biol. *296*, 385–401. https://doi.org/10.1006/jmbi.1999.3486.

48. Calì, S., Spoldi, E., Piazzolla, D., Dodd, I.B., Forti, F., Dehò, G., and Ghisotti, D. (2004). Bacteriophage P4 Vis protein is needed for prophage excision. Virology *322*, 82–92. https://doi.org/10.1016/j.virol.2004.01.016.
49. Ghisotti, D., Finkel, S., Halling, C., Dehò, G., Sironi, G., and Calendar, R. (1990). Nonessential region of bacteriophage P4: DNA sequence, transcription, gene products, and functions. J. Virol. *64*, 24–36. https://doi.org/10.1128/JVI.64.1.24-36.1990.
50. Shu, X., Wang, R., Li, Z., Xue, Q., Wang, J., Liu, J., Cheng, F., Liu, C., Zhao, H., Hu, C., et al. (2025). CRISPR-repressed toxin-antitoxin provides herd immunity against anti-CRISPR elements. Nat. Chem. Biol. *21*, 337–347. https://doi.org/10.1038/s41589-024-01693-3.
51. Makarova, K.S., Anantharaman, V., Aravind, L., and Koonin, E.V. (2012). Live virus-free or die: coupling of antivirus immunity and programmed suicide or dormancy in prokaryotes. Biol. Direct *7*, 40. https://doi.org/10.1186/1745-6150-7-40.
52. Olson, M.G., Goldammer, M., Gauliard, E., Ladant, D., and Ouellette, S.P. (2018). A Bacterial Adenylate Cyclase-Based Two-Hybrid System Compatible with Gateway® Cloning. Methods Mol. Biol. *1794*, 75–96. https://doi.org/10.1007/978-1-4939-7871-7_6.
53. Patel, I.R., Gangiredla, J., Mammel, M.K., Lampel, K.A., Elkins, C.A., and Lacher, D.W. (2018). Draft Genome Sequences of the Escherichia coli Reference (ECOR) Collection. Microbiol. Resour. Announc. *7*, e01133-18. https://doi.org/10.1128/MRA.01133-18.
54. Silas, S., Mohr, G., Sidote, D.J., Markham, L.M., Sanchez-Amat, A., Bhaya, D., Lambowitz, A.M., and Fire, A.Z. (2016). Direct CRISPR spacer acquisition from RNA by a natural reverse transcriptase-Cas1 fusion protein. Science *351*, aad4234. https://doi.org/10.1126/science.aad4234.
55. Yuping, L., Guan, L., Becher, I., Makarova, K.S., Cao, X., Hareendranath, S., Guan, J., Stein, F., Yang, S., Boergel, A., et al. (2025). Jumbo phage killer immune system targets early infection of nucleus-forming phages. Cell. https://doi.org/10.1016/j.cell.2025.02.016.
56. Wetmore, K.M., Price, M.N., Waters, R.J., Lamson, J.S., He, J., Hoover, C. A., Blow, M.J., Bristow, J., Butland, G., Arkin, A.P., and Deutschbauer, A. (2015). Rapid quantification of mutant fitness in diverse bacteria by sequencing randomly bar-coded transposons. mBio *6*, 10–1128. https://doi.org/10.1128/mBio.00306-15.
57. Peters, J.M., Koo, B.M., Patino, R., Heussler, G.E., Hearne, C.C., Qu, J., Inclan, Y.F., Hawkins, J.S., Lu, C.H.S., Silvis, M.R., et al. (2019). Enabling genetic analysis of diverse bacteria with Mobile-CRISPRi. Nat. Microbiol. *4*, 244–250. https://doi.org/10.1038/s41564-018-0327-z.
58. Mejia-Santana, A., Lloyd, C.J., and Klose, K.E. (2021). New cloning vectors to facilitate quick allelic exchange in gram-negative bacteria. BioTechniques *70*, 116–119. https://doi.org/10.2144/btn-2020-0135.
59. Jain, C., Rodriguez-R, L.M., Phillippy, A.M., Konstantinidis, K.T., and Aluru, S. (2018). High throughput ANI analysis of 90K prokaryotic genomes reveals clear species boundaries. Nat. Commun. *9*, 5114. https://doi.org/10.1038/s41467-018-07641-9.
60. Steinegger, M., and Söding, J. (2017). MMseqs2 enables sensitive protein sequence searching for the analysis of massive data sets. Nat. Biotechnol. *35*, 1026–1028. https://doi.org/10.1038/nbt.3988.
61. Eddy, S.R. (2011). Accelerated Profile HMM Searches. PLoS Comput. Biol. *7*, e1002195. https://doi.org/10.1371/journal.pcbi.1002195.
62. Langmead, B., and Salzberg, S.L. (2012). Fast gapped-read alignment with Bowtie 2. Nat. Methods *9*, 357–359. https://doi.org/10.1038/nmeth.1923.
63. Li, H., Handsaker, B., Wysoker, A., Fennell, T., Ruan, J., Homer, N., Marth, G., Abecasis, G., and Durbin, R.; 1000 Genome Project Data Processing Subgroup (2009). The Sequence Alignment/Map format and SAMtools. Bioinformatics *25*, 2078–2079. https://doi.org/10.1093/bioinformatics/btp352.
64. Quinlan, A.R., and Hall, I.M. (2010). BEDTools: a flexible suite of utilities for comparing genomic features. Bioinformatics *26*, 841–842. https://doi.org/10.1093/bioinformatics/btq033.
65. Tesson, F., Hervé, A., Mordret, E., Touchon, M., d'Humières, C., Cury, J., and Bernheim, A. (2022). Systematic and quantitative view of the antiviral arsenal of prokaryotes. Nat. Commun. *13*, 2561. https://doi.org/10.1038/s41467-022-30269-9.
66. Gilchrist, C.L.M., and Chooi, Y.-H. (2021). clinker & clustermap.js: automatic generation of gene cluster comparison figures. Bioinformatics *37*, 2473–2475. https://doi.org/10.1093/bioinformatics/btab007.
67. Martin, M. (2011). Cutadapt removes adapter sequences from high-throughput sequencing reads. EMBnet. j. *17*, 3. https://doi.org/10.14806/ej.17.1.200.
68. Jumper, J., Evans, R., Pritzel, A., Green, T., Figurnov, M., Ronneberger, O., Tunyasuvunakool, K., Bates, R., Žídek, A., Potapenko, A., et al. (2021). Highly accurate protein structure prediction with AlphaFold. Nature *596*, 583–589. https://doi.org/10.1038/s41586-021-03819-2.
69. Cook, R., Brown, N., Redgwell, T., Rihtman, B., Barnes, M., Clokie, M., Stekel, D.J., Hobman, J., Jones, M.A., and Millard, A. (2021). INfrastructure for a PHAge REference Database: Identification of Large-Scale Biases in the Current Collection of Cultured Phage Genomes. Phage (New Rochelle) *2*, 214–223. https://doi.org/10.1089/phage.2021.0007.

## STAR★METHODS

### KEY RESOURCES TABLE

| REAGENT or RESOURCE | SOURCE | IDENTIFIER |
|---|---|---|
| Antibodies | | |
| Rabbit anti-GST | Cell Signaling Technology | 91G1 |
| Mouse anti-FLAG | Sigma | F1804 |
| Anti-Rabbit HRP-linked IgG | Cell Signaling Technology | 7074S |
| Anti-Mouse HRP-linked IgG | Invitrogen | 62-6520 |
| Mouse anti-*E. coli RNAPβ* | Biolegend | 663903 |
| Bacterial and virus strains | | |
| ECOR 1-72 | STEC Center | N/A |
| *E. coli* MG1655 | Carol Gross' Lab Stocks | N/A |
| *E. coli* C990 | Ry Young | N/A |
| *E. coli* DH5alpha | NEB | C2987H |
| *E. coli* TOP10 | Thermo Fisher Scientific | C404010 |
| *E. coli* BW25113 | Vivek Mutalik | N/A |
| *E. coli* BW25141 | Jason Peters | N/A |
| *E. coli* WM6026 | Jason Peters | N/A |
| *E. coli* DHT1 | Olson et al.[52] | N/A |
| T2-T7 phages | Vivek Mutalik | N/A |
| Lambda-vir phage | Ry Young | N/A |
| Chemicals, peptides, and recombinant proteins | | |
| IPTG isopropyl-b-D-thiogalactopyranoside | VWR | 76800-062 |
| L-arabinose | VWR | TCA0515 |
| D-Glucose | VWR | 97061–166 |
| 2,6-diaminopimelic acid | Sigma Aldrich | 33240 |
| X-α-Gal, 5-Bromo-4-chloro-3-indolyl-α-D-galactopyranoside | Millipore Sigma | 16555 |
| Benzonase nuclease, recombinant | Sigma Aldrich | E1014 |
| Lysozyme, chicken egg white | VWR | AAJ60701-03 |
| cOmplete™ ULTRA Tablets, Mini, EDTA-free, EASYpack Protease Inhibitor Cocktail | Sigma Aldrich | 5892791001 |
| Pierce™ Glutathione Magnetic Agarose Beads | Thermo Fisher Scientific | 78602 |
| L-glutathione, reduced | Millipore Sigma | G4251 |
| Critical commercial assays | | |
| Genomic DNA Clean and Concentrator Kit | Zymo Research | D4065 |
| Gel DNA recovery Kit | Zymo Research | D4008 |
| Plasmid miniprep Kit - Classic | Zymo Research | D4054 |
| Illumina DNA prep kit | Illumina | 20060060 |
| NEB Ultra II FS DNA Library Prep Kit | NEB | E7805L |
| 2X Gibson assembly master mix | NEB | E2611L |
| NEBuilder HiFi DNA assembly master mix | NEB | E2621L |
| 1x dsDNA HS assay kit | Thermo Fisher Scientific | Q33231 |
| Luna® Universal One-Step RT-qPCR Kit | NEB | E3005L |
| AMpure XP beads | Beckman Coulter | A63881 |

(*Continued on next page*)

*Continued*

| REAGENT or RESOURCE | SOURCE | IDENTIFIER |
|---|---|---|
| **Deposited data** | | |
| Sequencing data | This paper | SRA: PRJNA952709 |
| ECOR strain genomes | USDA[53] | N/A |
| Imaging data | This paper | Mendeley Data: https://doi.org/10.17632/b722nfy9hv.1 |
| **Oligonucleotides** | | |
| JSW-SS-170 (Ns are mixed bases) CGACGCTCTTCCGATCTNNNNNT GATGTCGTTGTTGCCATCG | This paper | N/A |
| JSW-SS-171 ACTGACGCTAGTGCA TCACTTTCTGAGCCAGTGTTGCT | This paper | N/A |
| JSW-SS-42 – 53 (with X8 barcode) CAAGCAGAAGACGGCATACGAG AT(X8)GTGACTGGAGTTCAGACGT GTGCTCTTCCGATCTACTGACGC TAGTGCATCA | Silas et al.[54] | N/A |
| JSW-SS-54 – 61 (with X8 barcode) AATGATACGGCGACCACCGAGAT CTACAC(X8)ACACTCTTTCCCT ACACGACGCTCTTCCGATCT | Silas et al.[54] | N/A |
| YL001 /5Phos/GATCGGAAGAG/3ddC/ | Li et al.[55] | N/A |
| YL002-5 (with X4 barcode, Ns are mixed bases) AGCGGCAATTTCACACAGG ACAAGCAGAAGACGGCATACGAG ATNNNNNNNN(X4)GTGACTGGAG TTCAGACGTGTGCTCTTCCGATC*T | Li et al.[55] | N/A |
| YL006 AGCGGCAATTTCACACAGGA | Li et al.[55] | N/A |
| oAD493 ACACTGGC AGAGCATTACGCCCT | Wetmore et al.[56] | N/A |
| YL009 CAAGCAGAAGACGGCATACGAG | Li et al.[55] | N/A |
| JBD-SS-273 – 280 (with X8 barcode, Ns are mixed bases) AATGATACGGCGACC ACCGAGATCTACAC(X8)ACACTCTTTCC CTACACGACGCTCTTCCGATCTNNNN NNNGCAGGGATGTCCACGAGGTCTCT | This paper | N/A |
| **Recombinant DNA** | | |
| pJMP1039/pTn7C1 helper plasmid | Peters et al.[57] | N/A |
| pJMP1360/pTn7C185 transposon vector | Peters et al.[57] | N/A |
| pBAD Myc/His A vector | Thermo Fisher Scientific | V44001 |
| pKEK2201 | Mejia-Santana et al.[58] | N/A |
| phage AG CDs X 200 | Twist Biosciences | N/A |
| pJMP1360/pTn7C185::phage AGs X 200 | This paper | N/A |
| pKEK2201::Δ*wecA* allelic exchange vector | This paper | N/A |
| pBAD::Ronin | This paper | N/A |
| pBAD::ECOR22I | This paper | N/A |
| pBAD::Yemaya | This paper | N/A |
| pBAD::gop-beta-cII | This paper | N/A |
| pBAD::P4 | This paper | N/A |
| T18 and T25 fragments of *B. pertussis* adenylate cyclase | Twist Biosciences | N/A |
| APA766 (pKMW7-derived Tn5 transposon vector for RB-TnSeq) | Wetmore et al.[56] | N/A |

(*Continued on next page*)

*Continued*

| REAGENT or RESOURCE | SOURCE | IDENTIFIER |
|---|---|---|
| Software and algorithms | | |
| Phagent | This paper | https://github.com/sukritsilas/phagent |
| fastANI | Jain et al.[59] | https://github.com/ParBLiSS/FastANI |
| MMSeqs2 | Steinegger and Söding[60] | https://github.com/soedinglab/MMseqs2 |
| Hmmer (v3.4) | Eddy[61] | http://hmmer.org/ |
| Bowtie2 (v2.2.5) | Langmead and Salzberg[62] | https://bowtie-bio.sourceforge.net/bowtie2/index.shtml |
| SAMtools (v1.14) | Li et al.[63] | https://github.com/samtools/samtools/releases/ |
| BEDTools (v2.31.0) | Quinlan and Hall[64] | https://bedtools.readthedocs.io/en/latest/index.html |
| DefenseFinder | Tesson et al.[65] | https://github.com/mdmparis/defense-finder |
| Clinker | Gilchrist et al.[66] | https://github.com/gamcil/clinker |
| Cutadapt (v5.0) | Marcel Martin[67] | https://cutadapt.readthedocs.io/en/stable/ |
| AlphaFold2 | Jumper et al.[68] | https://colab.research.google.com/github/sokrypton/ColabFold/blob/main/AlphaFold2.ipynb |
| Other | | |
| Illumina MiSeq | Illumina | N/A |
| Illumina NextSeq | Illumina | N/A |
| Illumina NovaSeq | Illumina | N/A |

## EXPERIMENTAL MODEL AND STUDY PARTICIPANT DETAILS

The *E. Coli* Reference (ECOR) collection of wild *E. coli* strains was obtained from the STEC Center (Michigan State University). Lab strains were obtained as follows: MG1655 (from Dr. Carol Gross, UCSF), C990 (from Dr. Ry Young, Texas A&M), DH5α (NEB), DH10ß/TOP10 (Life Technologies), BW25113 (from Dr. Vivek Mutalik, LBNL), and BW25141 and WM6026 (from Dr. Jason Peters, UW-Madison). All strains were cultured at 37°C with shaking (180-225 rpm) in lysogeny broth (LB) (10 g/l tryptone, 5 g/l yeast extract, 10 g/l NaCl with 15 g/l agar for plates) supplemented with 100 μg/ml of ampicillin/carbenicillin, 10-20 μg/ml gentamicin (except WM6026, which yielded more consistent colony sizes with 50 μg/ml), 50 μg/ml kanamycin, and 0.5% w/v glucose, 0.1% w/v L-arabinose, and 1 mM IPTG (isopropyl-b-D-thiogalactopyranoside) as needed. The WM6026 strain required diaminopimelic acid (DAP) for growth, which was supplied at 300 μM. All strains were stored in 20% glycerol at -80°C for long term storage.

R6K-origin pTn7 plasmids (from Dr. Jason Peters, UW-Madison) – the pJMP1039/pTn7C1 helper plasmid (carbenicillin) and the pJMP1360/pTn7C185 transposon vector (gentamicin, carbenicillin) – were used for integration of phage AGs into the *E. coli* genome. All host defense systems identified in the various screens were placed under the araBAD promoter (arabinose inducible) in the pBAD Myc/His A vector (Invitrogen). Conjugative allelic exchange was carried out using R6K-origin pKEK2201 (kanamycin) (from Karl E. Klose, UT San Antonio). All plasmids were constructed by Gibson Assembly.

R6K-origin plasmids were maintained in BW25141 (routine cloning) and WM6026 (conjugative donor strain). All other plasmids were maintained in DH5α or TOP10. All plasmid sequences were verified by Sanger or whole-plasmid sequencing (Plasmidsaurus, Primordium) and are available upon request. Frequent plasmid dimerization during the Gibson Assembly procedure (especially when using the NEBuilder reagent) was ameliorated by using 10-fold less of one of the insert DNA fragments in a reaction involving at least 2 insert fragments (not including the backbone).

## METHOD DETAILS

### AG conjugation into host strains

AGs were delivered to *E. coli* hosts by Tn7 transposition via conjugation performed by triparental mating.[57] The transposon and helper plasmids were delivered to the recipient from WM6026 donor strains by overnight incubation on LB agar plates supplemented with 300 μM DAP and 0.5% glucose to repress AG expression. The next day, cells were scraped and resuspended in 1 ml LB, and 1000X-20000X dilutions of this conjugation mixture were plated on LB plates (lacking DAP) supplemented with the appropriate antibiotics and 0.5% glucose. All strains were maintained under strict glucose repression of the pLlacO-1 promoter at every step until screens

were performed. Thus, all AGs were maintained as single-copy chromosomal inserts at the same attTn7 site in the genomic region between *glmS* and *pstS* genes.

Efficient Tn7 transposition is necessary to construct an AG library in any given *E. coli* host. Tn7 conjugation-transposition efficiencies were determined in 44 ECOR stains containing an intact *glmS-pstS* region (we note that other strains can support Tn7 integration as well). Tn7 transposons carried only a barcode sequence and the gentamicin-resistance gene to minimize payload-dependent variation in conjugation efficiency between strains. Efficiency of conjugation was determined by streaking the conjugation mixture on two different gentamicin concentrations (25 μg/ml and 10 μg/ml) to account for possible differences in natural antibiotic resistance between the wild strains. The barcode sequence was verified by Sanger sequencing and both flanks were checked by PCR to ensure proper integration of the Tn7 transposon at the expected attTn7 site. Strains that supported Tn7 transposition at high levels and were amenable to agar-overlay plaque assays were selected for further experiments.

### DNA extraction and Nextera whole-genome sequencing

Genomic DNA was extracted using a modified SDS–proteinase K method: Briefly, cells pelleted from 50 μl of saturated culture (or 5 μl of the cell mixture scraped from selective plates during AG library construction) were re-suspended in 200 μl of lysis buffer (10 mM tris, 10 mM EDTA, 400 μg/ml proteinase K, 0.5% SDS) and incubated at 50-55°C for 1 hour. Subsequently, the temperature was lowered to 37°C and RNase A (Thermo Scientific) was added to a concentration of 1 mg/ml. After 30-60 min of incubation, the digests subsequently purified using the Genomic DNA Clean & Concentrator Kit (Zymo Research). DNA was prepared for whole-genome sequencing using the Nextera Flex Library Prep Kit (now, the Illumina DNA Prep Kit) according to manufacturer's instructions, except that we lowered the volumes of all tagmentation reactions 5-fold, and used a custom dual-indexed primer set JSW-SS-22:33 (CAAGCAGAAGACGGCATACGAGAT NNNNNNNN GTCTCGTGGGCTCGG) and JSW-SS-34:41 (AATGATACGGCGACCACCGA GATCTACAC NNNNNNNN TCGTCGGCAGCGTC) to amplify libraries for 11-13 cycles using Phusion High Fidelity PCR Master Mix (NEB) instead of the Illumina-supplied PCR reagents. The $N_8$ sequences correspond to reverse-complemented Nextera DNA indexes N701 to N712 and N501 to N508, respectively (Illumina). Libraries were resolved by agarose gel electrophoresis and DNA was excised in the 300-400 bp range. Gel slices were purified using the Zymo Gel DNA Recovery Kit and sequenced on the Illumina MiSeq using 150-cycle v3 or 600-cycle v2 reagent kits.

Sequencing adaptors were trimmed from reads using cutadapt, mapped to reference genomes using bowtie2, and visualized using IGV. Reference genomic contigs of ECOR strains were obtained from the USDA.[53]

### Phage propagation and plaque assays

High-titer phage stocks were generated by growth in liquid culture. All phage infections were performed at 37°C in LB supplemented with 10 mM $MgSO_4$ and 5 mM $CaCl_2$. *E. coli* BW25113 or C990 were grown to an optical density (at 600 nm; $OD_{600}$) ~0.5 (1-5 X $10^8$ cfu/ml) and infected with the desired phage at MOI ~5. Infections were allowed to proceed at 37°C with agitation for 5-6 hours until the cultures were clear. Lysates were clarified by centrifugation (8000 X g for 2 min) and sterile-filtered using a 0.45 μm SFCA syringe filter (Millipore). Phage lysates were stored at 4°C.

Bacteriophages T2, T3, T4, T5, T6, T7, P1vir were obtained from Dr. Vivek Mutalik (LBNL), and λvir was obtained from Dr. Ry Young (Texas A&M). To the extent possible, all phages were grown on *E. coli* C990 which lacks restriction-modification. T4 and P1vir could not be grown on C990 and were instead grown on *E. coli* BW25113. To ensure that our phage lysates were free from ancestral Type I R-M methylation marks or other host-passage derived DNA modifications, we serially passaged all phages in the desired hosts 3 times. All phage genomes were subsequently verified by Nextera high-throughput sequencing.

Phage titers were determined against various hosts by the agar-overlay method with LB top agar containing 0.7% agar, 10 mM $MgSO_4$ and 5 mM $CaCl_2$. Phage spot-titration assays were performed with 10-fold serial dilutions of phage lysates (3-5 μl of each dilution pipetted onto bacteria immobilized in top-agar overlay using a multichannel pipette).

### AG library preparation and NGS verification for testing post-conjugation evenness

200 AGs with unique 10 bp DNA barcodes were synthesized (Twist and IDT) and cloned individually under pLlacO-1 control (IPTG inducible, repressed by glucose) into a modified pTn7C185 vector (with mobile CRISPRi components sgRNA and dCas9 removed). Plasmid assembly reactions were performed in 96-well format using the 2X Gibson assembly master mix (NEB) and transformed into chemically competent BW25141 cells in 96-well format. Transformations were individually plated on LB agar supplemented with 20 μg/ml gentamicin and 0.5% glucose and one colony was initially checked by Sanger sequencing from each plate. Where a successful transformant could not be obtained on the first attempt, more colonies were sequenced in successive rounds until a plasmid with no mutations in the region spanning the pLlacO-1 promoter, the AG ORF, and the barcode sequence was obtained. Verified vectors were miniprepped using the ZR Plasmid miniprep – Classic kit (Zymo) and transformed into chemically competent WM6026 cells in 96-well format, and each transformation was plated individually on LB agar supplemented with 50 μg/ml gentamicin, 300 μM DAP, and 0.5% glucose.

One colony from each of the 200 WM6026 transformants was grown in 2 ml square-well 96-well plates with shaking overnight, and 100 μL of each culture was then pooled together to yield ~20 ml of the donor mixture. This mixture was concentrated down to 10 ml by centrifugation at 6000 g for 10 min, and 5 ml of 60% glycerol (20% final) was added to yield the donor library. The 15 ml library was divided into single-use 50 μL aliquots (each containing >50M cells, i.e. >300K of each donor strain) and stored at -80°C.

Genomic DNA was extracted from one of the library aliquots and all constructs in the final pool were verified by Nextera high-throughput sequencing. This allowed us to assess library evenness as well as verify the fidelity of our cloning, colony picking, and strain pooling process. Overall, 195 AGs were cloned successfully. One AG (*orf88*) never yielded any colonies in multiple cloning attempts, possibly due to its cytotoxicity. Three AGs (*orf36, orf52, orf94*) were dropouts during the WM6026 growth step, and another two (*orf25, orf84*) were discovered to contain mutations upon high-throughput sequencing that had been missed by Sanger sequencing. *Orf25* had previously presented difficulties in cloning, and did not yield a mutation-free construct even after checking >12 colonies (whereas most transformations yielded a correct construct on the first attempt). The *orf84* construct contained a mixed base at the last position of the second repeat of the Lac-operator sequence upstream of the ORF, which would not be expected to affect any downstream assays significantly.

The donor library was conjugated into MG1655 *E. coli* according to the Tn7 transposition procedure (above) and a 1000X dilution of the conjugation mixture was plated on LB agar supplemented with 20 μg/ml gentamicin and 0.5% glucose. We routinely use multiple 150 mm X 15 mm bacteriological petri dishes (Corning) to obtain sufficient numbers of transconjugant colonies to assemble libraries. The next day, >>2,000-20,000 transconjugant colonies (10-100X the number of AGs in the library) were scraped and combined thoroughly, and the thick cell mixture was directly frozen at -80°C in 20% glycerol. Genomic DNA was extracted from this mixture and the distribution of DNA barcodes corresponding to individual AGs was measured in both this post-conjugation strain mixture as well as the genomic DNA extracted from the WM6026 donor library aliquot.

To amplify barcodes for high-throughput sequencing, genomic DNA was subjected to two successive rounds of PCR. The DNA barcodes were amplified from genomic DNA using universal primers JSW-SS-170 (CGACGCTCTTCCGATCTNNNNN TGAT GTCGTTGTTGCCATCG) and JSW-SS-171 (ACTGACGCTAGTGCATCA CTTTCTGAGCCAGTGTTGCT) and the Q5 Hot Start High-Fidelity 2X PCR master mix (NEB) according to manufacturer's instructions. Sequencing adaptors were attached in a second round of PCR using amplicons from the first PCR round as the templates, with dual-indexed primer sets JSW-SS-42:53 (CAAGCAGAA GACGGCATACGAGAT NNNNNNNN GTGACTGGAGTTCAGACGTGTGCTCTTCCGATCT ACTGACGCTAGTGCATCA) and JSW-SS-54:61 (AATGATACGGCGACCACCGAGATCTACAC NNNNNNNN ACACTCTTTCCCTACACGACGCTCTTCCGATCT), where the $N_8$ sequences correspond to reverse-complemented TruSeq HT indexes D701 to D712 and D501 to D508, respectively (Illumina). Template-matching regions in the primers are underlined. Cycling conditions for round 1 were as follows: one cycle at 98°C for 1 min; two cycles at 98°C for 10s, 66°C for 30s, and 72°C for 10s; 22 cycles at 98°C for 10s, and 72°C for 20s; and one cycle at 72°C for 2 min. Conditions for round 2 were one cycle at 98°C for 1 min; two cycles at 98°C for 10 s, 64°C for 30 s, and 72°C for 10 s; 4 cycles at 98°C for 10 s, and 72°C for 20 s; and one cycle at 72°C for 2 min. 0.5-1 μL of unpurified 1$^{st}$ round reaction product was used as template for the 2$^{nd}$ round of PCR. Amplicons from the 2$^{nd}$ round were gel-purified by electrophoresis (3% agarose gel, 4.2 V/cm, 2 hours) and quantified using the 1X dsDNA HS kit with the Qubit 4.0 Fluorometer (Invitrogen). Amplicons were sequenced on a MiSeq using the 150-cycle v3 reagent kit (Illumina) in single-end format (100 bp) with two (8 bp) index reads. DNA barcodes were trimmed from the reads and the proportions of various AGs in the mixtures were determined using the prevalence of the corresponding barcode sequence.

Concordance between the Nextera whole-genome sequencing and the barcode sequencing of the WM6026 donor mixture showed that barcode representation was a suitable proxy for the true distribution of AGs in the mixture and that amplification biases during library preparation were not a significant source of noise. Concordance between barcode sequencing in the WM6026 donor and MG1655 post-conjugation recipient mixtures indicated that the Tn7 transposition and colony scraping process does not meaningfully bottleneck AG distribution.

The AG library was then conjugated (in triplicate) into ECOR strains that were previously confirmed to support robust Tn7 transposition. Strain mixtures were prepared in a procedure analogous to library construction in MG1655, except higher dilutions of the ECOR+AG conjugation mixtures (10,000-20,000X) were plated and the gentamicin concentration on selective plates was lowered to 10 μg/ml to account for higher steady-state cell densities and higher gentamicin sensitivity of the wild *E. coli* strains. As with the MG1655 library, thick cell mixtures comprised of >>2,000-20,000 colonies scraped from each replicate conjugation were directly stored at -80°C in 20% glycerol and used to seed cultures for the AG screens (below). Genomic DNA was extracted from each mixture and barcode sequencing was performed to measure the AG distribution in every replicate of all ECOR strain derived libraries. The replicates were very highly correlated, and AG distributions in all libraries were confirmed to be free of significant bottlenecking. These datasets are the reference libraries that serve as the baseline for AG induction experiments.

## AG screen

Thick cell mixtures from each of the three replicates of the various ECOR+AG libraries were thawed on ice and diluted into LB supplemented with $Mg^{2+}$, $Ca^{2+}$, and 10 μg/ml gentamicin. Typically, 1-5 μl of the library mixture was diluted in 2 ml broth to yield an initial $OD_{600}$ of 0.1-0.15. The cultures were immediately split x2, with one tube used to monitor $OD_{600}$ values as the experiments progressed, and the other left untouched for the screen. AG expression was induced by the addition of 1 mM IPTG after acclimatization for 15 min at 37°C in a shaking incubator and $OD_{600}$ values were measured again for each ECOR+AG library at time of induction. Parallel uninduced controls were maintained throughout the experiment. Libraries were then grown for ~80-120 min depending on the relative growth rates of the various ECOR strains, to $OD_{600}$ ~1.2-1.5. A $10^{-5}$ dilution of each late-log phase culture was then plated on LB agar (with 10 μg/ml gentamicin and 0.5% glucose to repress AGs and avoid fitness costs) to obtain a count of viable colony forming units (cfu). Cultures were immediately diluted ~1:20 in fresh LB (with IPTG, $Mg^{2+}$, $Ca^{2+}$, and 10 μg/ml gentamicin) and 1 ml aliquots were allowed to grow for another 30-60 min. After the induction period was complete, the cultures were vortexed,

diluted 1:100, vortexed again, and 50 μl of the dilution was plated on 2 large (150 mm X 15 mm) LB agar plates (with 10 μg/ml gentamicin and 0.5% glucose to repress AGs and avoid fitness costs). The next day >>2,000-20,000 colonies were scraped from each set of plates. 5 μl of the thick resulting cell mixtures was reserved for genomic DNA extraction, and the rest was frozen at -80°C in 20% glycerol as a backup.

AG barcodes were amplified and sequenced as with the WM6026 donor library, with a slight modification. The three biological replicate sets of ECOR+AG experiments were amplified using JSW-SS-171 and different versions of primer JSW-SS-170 containing extra N's at the start of the sequencing read. The first replicate was amplified with JSW-SS-170 (containing 5 N's), the second replicate with JBD-SS-254 (CGACGCTCTTCCGATCTNNNNNN TGATGTCGTTGTTGCCATCG) with 6 N's, and the third replicate with JBD-SS-255 (CGACGCTCTTCCGATCTNNNNNNN TGATGTCGTTGTTGCCATCG) with 7 N's. This ensured that reads from the three sets would not cross contaminate analyses of replicate experiments. Amplicons were sequenced to the same depth as the baseline libraries on Illumina MiSeq and NextSeq instruments in single-end format (100 bp) with two (8 bp) index reads.

### RB-TnSeq Tn5 library construction

Tn5 whole-genome knockout strain libraries were constructed using the RB-TnSeq donor library (pKMW7-derived strain APA766 from Dr. Adam Deutschbauer) conjugated with the recipient ECOR strain in a biparental mating on LB plates supplements with 300 μM DAP. The next day, cell mixtures were scraped and resuspended in 1 ml LB and 1000X dilutions of this conjugation mixture were plated on 10 large (150 mm X 15 mm) LB plates (lacking DAP) supplemented with 50 μg/ml kanamycin. Approximately 0.5-1 million colonies were scraped taking care to break colonies apart on the surface of the plates, mixed very thoroughly, aliquoted, and stored at -80°C with 20% glycerol, with ~5-10 μl reserved for genomic DNA extraction and reference library preparation.

RB-TnSeq allows the same mutant library to be challenged under various conditions and simplifies the downstream sequencing-library preparation by substituting barcode sequencing for all experimental conditions after initial characterization of the reference library. For completeness, we describe the RB-TnSeq procedures here as implemented in our lab.

To characterize the Tn5-knockout reference libraries in the various ECOR strains, genomic DNA was extracted from 5-10 μl of the cell scrape and prepared for sequencing using the NEBNext Ultra II FS DNA Library Prep Kit (NEB) with the following modifications. 500 ng DNA was fragmented for 25 min according to manufacturer's instructions. The adaptor ligation step was performed as directed albeit with a custom pre-annealed oligo adaptor comprising of YL001 (/5Phos/GATCGGAAGAG/3ddC/) annealed to one of YL002:005 (AGCGGCAATTTCACACAGGACAAGCAGAAGACGGCATACGAGATNNNNNNNNAGTGGTGACTGGAGTTCAGACGT GTGCTCTTCCGATC*T) where the 4-base underlined sequence serves as a variable barcode unique to each oligo. The USER Enzyme steps post-ligation were skipped and the bead-cleanup was performed using 40 μl and 20 μl of Sample Purification Beads successively as instructed for library size selection in the 150-250 bp range. The PCR amplification of transposon-genome junctions was performed using the cycling parameters described in the kit for 11 cycles with Q5 Ultra II FS Master Mix (NEB) using primers YL006 (AGCGGCAATTTCACACAGGA) and JBD-SS-272/oAD493 (ACACTGGCAGAGCATTACGCCCT) instead of the kit-supplied primers. A second nested-PCR enrichment step was performed for 11 cycles using the same cycling parameters as before, using the entire bead-purified reaction product from the first step as a template with primers YL009 (CAAGCAGAAGACGGCATACGAG) and JBD-SS-273:280 (AATGATACGGCGACCACCGAGATCTACAC TATAGCCT ACACTCTTTCCCTACACGACGCTCTTCCGATCT NNNNNNN GCAGGGATGTCCACGAGGTCTCT) where $N_8$ barcodes correspond to reverse-complemented Illumina TruSeq HT D501-508 indexes. Bead-purified amplicons were quantified using the 1X dsDNA HS kit with the Qubit 4.0 Fluorometer (Invitrogen) and sequenced on Illumina MiSeq and NovaSeq instruments in single-end format (150 bp) with two (8 bp) index reads.

### Tn5 suppressor screen to find abortive loci

Tn5 whole-genome knockout strain libraries were constructed using the RB-TnSeq donor conjugated with the recipient ECOR strain as described above in the RB-TnSeq procedure, with slight modifications. The recipient ECOR strain was equipped with the AG (as a single copy chromosomal Tn7 insertion as usual) which triggers PCD, presumably by activating an abortive defense system. The trigger AG was inserted prior to Tn5 library construction in order to minimize passages of the library prior to screening and avoid potential bottlenecking due to fitness effects of the various Tn5 knockouts. Libraries were constructed as above, except that conjugation was carried out under strict glucose repression to prevent PCD activation at this stage, and the conjugation mixture scraped from the LB+DAP+glucose plates was then plated directly on LB plates containing 10 μg/ml gentamicin and 1 mM IPTG in addition to 50 μg/ml kanamycin. We typically needed to plate the entire conjugation mixture scraped from five 100 mm LB+DAP+glucose plate onto five 150 mm LB+IPTG+Kan+Gm plate in order to obtain sufficient numbers of suppressor colonies for characterization by high-throughput sequencing. Control samples were obtained by plating 1000-2000X dilutions on LB+glucose+Kan+Gm plates. Suitable dilutions were empirically determined for the various ECOR hosts. The next day, suppressor colonies were scraped from the large plates and stored at -80°C with 20% glycerol, with ~5-10 μl reserved for genomic DNA extraction and sequencing. Genomic DNA was extracted and libraries were prepared and sequenced akin to the treatment of the RB-TnSeq/NEBNext reference libraries detailed above. There was no need for barcode sequencing since the screen identifies survivors instead of dropouts, and each library was only characterized once after IPTG induction/selection for suppressor mutants.

### Verification of abortive loci activity

Abortive/PCD systems identified by transposon screening of conditionally lethal AGs were cloned by Gibson assembly using the NEBuilder HiFi DNA assembly master mix (NEB) onto pBAD Myc/His A vectors along with their native promoters wherever possible. AGs that trigger PCD systems (or appropriate controls) were conjugated into DH10ß/TOP10 strains carrying pBAD-PCD plasmids using the Tn7 transposition method (above). Where the restriction/PCD systems prevented conjugation of AGs, the order of transformations was reversed – the AG was conjugated into naïve DH10ß/TOP10 cells first, and subsequently these strains were transformed with the pBAD-PCD vectors. Successful transconjugants were grown overnight with glucose to repress trigger AGs, and viability was tested the next day by spotting 10-fold serial dilutions of saturated cultures on LB agar plates with four additives: 1) Glucose repression to assess background toxicity, (2) Arabinose induction of PCD systems alone to assess fitness costs of over-expression of abortive components without the trigger AGs, (3) IPTG to assess ability of AGs to trigger PCD without over-expression of abortive components (i.e. under leaky expression conditions, or when expressed from the native promoters where present), and (4) IPTG and Arabinose to assess ability of AGs to trigger PCD when abortive components were also over-expressed.

### Verification of PCD by abortive systems

PCD was distinguished from dormancy as the mechanisms of growth inhibition by ECOR22I and Ronin by transient expression of the trigger AGs (30-120 min as indicated in figures) followed by plating on Glucose plates to test whether cells could be resuscitated once AG expression was shut off. For transient expression, late log phase cultures (1:20 dilution from overnight cultures into fresh LB, grown at 37°C for 2-3 hours) were induced by the addition of 1mM IPTG and incubated further for the indicated duration. Serial dilutions were then plated on plates containing Glucose (AGs repressed after transient activation) to measure cell killing, or IPTG (sustained AG activation) as a control to ensure the abortive systems were still functional.

### Co-immunoprecipitation of RonA and HsdS

Cells were collected from a saturated overnight culture of an *E. coli* TOP10 strain carrying a plasmid-encoded dual-tagged FLAG-*ronA hsdS*-GST version of Ronin, and whole-cell lysates were prepared by resuspending cell pellets in 1 mL lysis buffer (50mM Tris pH 7.4 at 4°C, 150mM NaCl, 10mM EDTA, 1mM $MgCl_2$, 0.5% NP40, 125 U/mL benzonase, 1x protease inhibitor cocktail (Roche, complete ULTRA mini EDTA free), 0.5 mg/ml lysozyme, 5 mM DTT for GST), incubating on ice for 1 hr, and sonicating with the samples continuously immersed in an ice-water slurry. Sonication was performed with a QSonica probe sonicator for a total of 2 min (2 sec ON, 10 sec OFF, for a total of 12 min at 20% amplitude).

Whole-cell lysates were incubated with magnetic glutathione agarose beads (Pierce) overnight at 4°C according to the manufacturer's instructions. Beads were then washed 2x in batch format with wash buffer 1 (50mM Tris pH 7.4, 150mM NaCl, 10mM EDTA, 1mM $MgCl_2$, 0.05% NP40) and then 3x with wash buffer 2 (same as wash buffer 1 but without detergent). Bound protein was eluted with 50mM reduced glutathione prepared immediately before use in wash buffer 2 and adjusted for pH. Western blotting of cell lysates and eluates was performed as follows. Samples were heated at 95°C for 5 min with 4x Laemmli buffer supplemented with ß-mercaptoethanol, resolved by SDS-PAGE, and transferred to PVDF membranes using the Bio-Rad Trans-Blot Turbo Transfer System according to the manufacturer's instructions. Membranes were blocked for 1 hr in blocking buffer (5% w/v solution of non-fat dry milk in TBS-T: 1X Tris-buffered saline (20 mM Tris, 150 mM NaCl) supplemented with 0.1% Tween-20 detergent). Membranes were then incubated with a primary antibody (Rabbit anti-GST (Cell Signaling Technology 91G1) diluted 1:2500, or Mouse anti-FLAG (Sigma F1804) diluted 1:1000 in blocking buffer for 1 hr, washed 3x with 25 mL TBS-T, then incubated with a secondary antibody (Anti-Rabbit HRP-linked IgG (Cell Signaling Technology 7074S) diluted 1:2000, or Anti-Mouse HRP-linked IgG (Invitrogen 62-6520) diluted 1:2000) for 1 hr, and washed 3x again with 25 mL TBS-T per wash. Membranes were developed using the Clarity Western ECL substrate kit (Bio-Rad) and imaged on an Azure bio-imaging system.

### Bacterial two-hybrid assay

The Bacterial Two-Hybrid Assay was performed as described previously.[52] *Bordetella pertussis* adenylate cyclase fragments T25 and T18 were synthesized by Twist Biosciences using sequences provided by Dr. Daniel Ladant (Insitut Pasteur). The Δcya *E. coli* strain DHT1 was provided kindly by Prof. Scot Oullette (University of Nebraska Medical Center).

### Live-cell and super-resolution microscopy

For live-cell microscopy, cells were immobilized under an LB agarose pad prepared with 0.064 g of agarose melted in a mixture of 2 mL LB and 6 mL $H_2O$ and poured onto assembled slides. Overnight bacterial cultures were diluted 1:100 into fresh LBM and grown at 37 °C with aeration at 300 rpm until the optical density at 600 nm ($OD_{600}$ reached approximately 0.4. Where necessary, AGs were pre-induced with 1 mM IPTG for 30 min immediately before imaging. Next, 1 μL of the bacterial cell suspension was placed onto an agarose pad, and the slide was assembled for imaging. Microscopy was performed using an inverted epifluorescence Ti2-E microscope (Nikon, Tokyo, Japan) equipped with the Perfect Focus System (PFS) and a Photometrics Prime 95B 25-mm camera. Image acquisition and processing were carried out with Nikon Elements AR software.

For single-molecule super-resolution microscopy, overnight cultures were diluted 1:100 in LB supplemented with 0.1% L-arabinose to overexpress Ronin, and grown until they reached an optical density (OD600) of 0.4–0.6. Cultures were induced with 1 mM IPTG for 30, 90 or 120 minutes before harvesting for microscopy. Cells were washed once with 1X phosphate buffer saline

(PBS) and resuspended in 700 μL of 1X PBS. Next, 30 μL of cell suspension were loaded onto a polylysine (Sigma P8920) coated coverslip and fixed in 4% paraformaldehyde for 10 minutes at room temperature. To minimize nonspecific staining, the sample was blocked with 5% BSA for 15 minutes at room temperature. To visualize the membranes, samples were stained with 10 μg/mL WGA AF647 in 1X PBS for 15 minutes, and washed three times with 1X PBS. ONI dSTORM imaging buffer was added prior to imaging.

Cells were imaged with an ONI NanoImager microscope (Oxford, UK). The microscope was equipped with 100x oil immersion objective with a numerical aperture of 1.45 and lasers with the following specifications: 405 nm/150 mW, 488 nm/1 W, 560 nm/500 mW, and 640 nm/1 W. ONI Bcube B dSTORM buffer was used as the imaging buffer. mNeonGreen was excited with a 488 nm laser at 112 mW, while WGA AF647 was excited using a 640 nm laser at 100 mW of power at the objective. Emission channels were separated using 640 dichroic and recorded as two separate images. Simultaneous excitation of dyes was performed with a 30 millisecond exposure time over 20,000 frames, employing HILO (Highly Inclined and laminated Optical sheet) illumination technique. The acquisition was performed using NimOS 19.5 software, which incorporates real-time localization to generate super-resolution images. To enhance image quality, NimOS built-in drift correction was applied to single molecule images, and a localization precision filter between 0 and 20 nm was employed. Additionally, the first 100 frames were disregarded to ensure stability before analysis. For analysis of the localization distribution, the line histogram tool available in NimOS was utilized to extract the localization across the width of 30 randomly selected cells. The resulting localization distribution over distance data were exported as a.CSV file for further analysis using GraphPad Prism 10.

### Timecourse measurements of Ronin transcription and translation

Two *E. coli* TOP10 strains with or without a chromosomal Tn7 insertion encoding IPTG-inducible *ardA*, both carrying a plasmid with the dual-tagged FLAG-*ronA hsdS*-GST version of Ronin were grown under glucose repression to mid-log phase (1:100 dilution of overnight cultures into 20 mL fresh LB + 0.5% glucose with the appropriate antibiotics, grown at 37°C for 2-3 hours), centrifuged gently at 6000 X g for 8 min, and resuspended in a 3x reduced volume (6 mL) of fresh LB to concentrate cells. Immediately, parallel aliquots were prepared for RNA extraction (100 μL) and preparation of whole cell lysates (1 mL) for analysis of protein production in the same sample. The 100 μL aliquot for RNA-extraction was immediately frozen on dry ice, and the 1 mL aliquot for protein analysis was immersed in an ice-water slurry until the end of the experiment when cells were spun down at >20000 X g and pellets were frozen. After the t=0 aliquot was saved, 1mM IPTG was added to both cultures and they were placed in a 37°C shaking water bath. Aliquots were then saved at 5, 10, 20, and 30 minutes after IPTG addition.

RNA was extracted using a hybrid Trizol-RNeasy method. Cells were scraped from plates and homogenized directly in 1 mL TRIZOL (Life Technologies) by vortexing and total RNA was extracted with 200 μL chloroform. 500 μL ethanol was added to an equal volume of the aqueous phase containing RNA, and the mixture was purified using the RNeasy Kit (QIAGEN) with On-Column DNase digestion according to the manufacturer's instructions. This protocol selects RNA >200-nt. Whole cell lysates were prepared as described above. Proteins were analyzed by western blotting with whole cell lysates as described above. RNAPß was used as a loading control, visualized with the Mouse anti-*E. coli RNAPβ* (Biolegend 663903) diluted 1:1000) primary antibody.

## QUANTIFICATION AND STATISTICAL ANALYSIS

### Computational pipeline to identify phage accessory regions

1706 non-redundant Enterobacteriophage genomes were obtained in September 2020 (from Dr. Andrew Millard, visit https://millardlab.org for current versions of this database[69]). These phages were both lytic and lysogenic but were sequenced and assembled from cultured isolates. Prophages and metagenomic samples were not included as it can be difficult to identify (pro)phage termini in these databases and many AGs could be early-expressed and located near genome ends. The database was limited to high-quality phage isolate genomes to maximize fidelity in AG selection as screening experiments would be performed only with a small subset of all phage AGs in Enterobacteria. All annotated protein sequences from all the phages were assigned unique numeric IDs and clustered by MMseqs2.[60] ORF IDs in phage genomes were then replaced by their MMseqs2 cluster representative IDs in each genome. Thus, each phage genome can be represented as an ordered list of IDs of clustered proteins. The gene-neighborhood of every ORF (up to 10 genes upstream and downstream) was extracted from every virus. Given that phage genomic termini can be difficult to identify accurately, every genome was considered potentially circularly permuted. Allowing for circularization also ensures that putative ARs towards ends of genomes would not be missed. A 2D matrix of all possible pairwise combinations of ORF IDs was constructed, with every matrix position containing lists of (a) the phages that each ORF appears in, (b) the 10 upstream, and (c) 10 downstream neighboring ORFs of each gene in every genome. We then traversed the matrix and assessed every ORF pair to identify all possible ARs, defined as the region between a pair of ORFs that are both present in at least 6 phage genomes but are no more than 10 genes apart in any genome. Hence, every virus genome that contained both ORFs of the pair was assigned to a virus cluster, and genes encoded between the query ORF pair were considered members of a candidate AR. Regions containing the same genes in every participating genome were discarded. Genomes containing a putative AR were then compared pairwise at the nucleotide level using FastANI[59], and ARs found in clusters of divergent phage genomes (<85% ANI) were removed. In practice, this was done by pre-computing an all-vs-all matrix of genome ANI, and then traversing subsets of the matrix with all the genomes containing a given putative AR to ensure no cells were empty (FastANI produces no output when highly divergent genomes are compared). Various

parameters were extracted from the retained candidate ARs. *N* is the number of unique genes in the AR. The vector *c* contains conservation numbers (the number of different genomes that each gene appears in; also indicated on top of each gene) for all the unique genes in this AR. The vector *l* contains the lengths (numbers of genes) of the AR in each genome. *CV* denotes coefficient of variation. *GCdev* is a vector containing one minus the absolute deviation of the GC content of each accessory gene from its resident genome. A scaling factor is also included to normalize the score by the number of phage genomes in the group that encompass at least one gene of the AR. ARs were scored according to the formula below.

$$ARscore = \frac{N * median(GCdev) * CV(c)}{CV(l) * mean(c)} * \frac{\#non\_empty}{\#genomes}$$

To filter out ARs that were subsets of other ARs, redundant, low scoring ARs with at least 90% of genes that had already been encountered in higher scoring ARs were successively removed. The top 200 ARs were examined manually and 1-15 AGs were selected from 62 ARs (Document S2 and Data S1 and S2). The code (with a readme and sample input files) is provided at https://github.com/sukritsilas/phagent.

## Runtime performance

The computational pipeline was benchmarked using a collection of 9451 non-redundant isolate bacteriophage genomes (assembled from NCBI Virus, RefSeq, IMG_VR, and PhageDB ca. 2020) in addition to the 1706 non-redundant Enterobacteriophage genomes. The maximum memory requirements of the accRegionMatrixConstructor.py program scaled from 1.008 GB to 5.682 GB between the 1706 and 9451 genome datasets (as calculated by the resource.getrusage(resource.RUSAGE_SELF) function), and the entire pipeline took 74 min to complete with the larger 9451 genome set on a Dell PowerEdge R6625 Server with 2 x 32 core / 64 thread AMD EPYC 9354 3.25 Ghz 256 MB cache (280W) processors, and 4800 MT/s DDR5 RAM. The majority of the runtime was dedicated to creating the phage genome similarity matrix using fastANI. The code was run in Python 3.6.8, with biopython 1.79, and pandas 1.1.5 as dependencies.

## AG screen data analysis

We required exact matches for the 20 bp primer-derived invariant sequences flanking the barcodes. These sequences were trimmed and the proportions of various AG-encoding strains in the mixtures were determined using the prevalence of the corresponding 10 bp barcode sequences. Barcode counts per AG were normalized by dividing each count by the median of each experiment, which would represent neutral AG fitness. A $\log_2$ transformation was subsequently applied to obtain fitness scores. Care was taken to sequence each library to similar depth such that fitness scores across experiments were distributed in the same range. Poorly represented AGs were identified in the baseline libraries as well as the induced experimental samples using a low read cutoff of 100, or if the $\log_2$ normalized average read counts across the three replicates for any AG were >3x the median absolute deviation below the median for that experiment. Reproducibility was determined using t tests across the three replicates, and we enforced a P-value cutoff of 0.2. The magnitude of the AG fitness effect was determined by subtracting the AG fitness scores in the baseline library from the induced libraries to assess whether AGs change host fitness. AGs were selected for further study if they were not poorly represented to begin with, produced reproducible effects across replicates, and changed host fitness by at least 4-fold.

Conditional lethal AGs were identified directly from the heatmap of fitness scores, with a subset selected for further experimentation using an arbitrary fitness cutoff of ~6-7 (i.e. ~100-fold).

## RB-TnSeq data analysis

The first 100 bp of these reads contain transposon derived sequences and a DNA barcode that uniquely identifies a particular Tn5 insertion. The last 50 bp of these reads contain host-genome derived sequence that help determine the location of the transposon insertion and hence construct a map between the Tn5 barcode and the insertion site (IS) in the genome. Briefly, 20 bp barcodes and 16-50 bp IS sequences were trimmed from the sequencing reads. To isolate the barcode and IS, we allowed 3 mismatches in the 23 bp invariant sequence upstream and up to 6 mismatches in the 50 bp downstream of the barcode using a Hamming distance function to compare the expected and actual sequences. Any reads failing these sequence-fidelity requirements were discarded. Reads containing an IS that matched the Tn5 transposon vector in the donor strain were also discarded. The 4 Ns adjacent to the underlined index sequences in YL002:005 were also sequenced as part of one 8 bp index read and served as a tag to remove PCR duplicates. This allowed us to distinguish between sequencing "reads" and DNA "fragments" present in the sample at the adaptor ligation step. Thus, reads containing unique combinations of barcode, PCR tag, and IS were entered into the barcode/IS map for each Tn5 library, each representing a distinct DNA fragment (but also machine errors in sequencing, chimeric PCR amplicons, 3′ truncations etc.). The filtered ISs were then mapped to genes within their respective host genomes. As described previously,[56] it is possible for transposon barcodes to map to the genomes ambiguously. Barcodes associated with multiple distinct ISs were retained only if their most frequently represented IS accounted for over 90% of the fragments containing that barcode. We then counted the number of DNA fragments recovered per gene.

### Tn5 suppressor screen data analysis

The number of transposon insertions (i.e. the number of uniquely mapping ISs from distinct DNA fragments) recovered per gene were used directly as a measure of survival of mutants despite expression of PCD-triggering AGs. In practice, no statistical analysis was necessary to identify the genetic loci responsible for PCD, as the signal-to-noise ratio was sufficiently high to allow visual identification of hits when transposon insertion frequency was plotted in control vs experimental samples (i.e. when the trigger AG was repressed by plating on glucose-containing media, vs induced with IPTG).

### Comparative analysis of Ronin systems

The *ronA* nucleotide sequence in the ECOR55 Ronin system was used as the query to identify similar genes by BLASTN. *RonA*-encoding bacterial genomes were downloaded using the entrez direct e-utilities command line tools. Of 100 complete genomes retrieved, *ronA* homologs had been annotated in 84. *hsdR* genes and other Type I R-M components were identified using phmmer and Defense Finder,[65] respectively. Ronin-adjacent genetic architectures were visualized using Clinker.[66] All ronin-adjacent architectures are shown in HTML files in Data S6 with mouse-over annotations for genes.

**Molecular Cell, Volume *85***

## Supplemental information

# Activation of bacterial programmed cell death by phage inhibitors of host immunity

**Sukrit Silas, Héloïse Carion, Kira S. Makarova, Eric S. Laderman, Thomas Todeschini, Pradeep Kumar, Matthew Johnson, Michael Bocek, Franklin L. Nobrega, Eugene V. Koonin, and Joseph Bondy-Denomy**

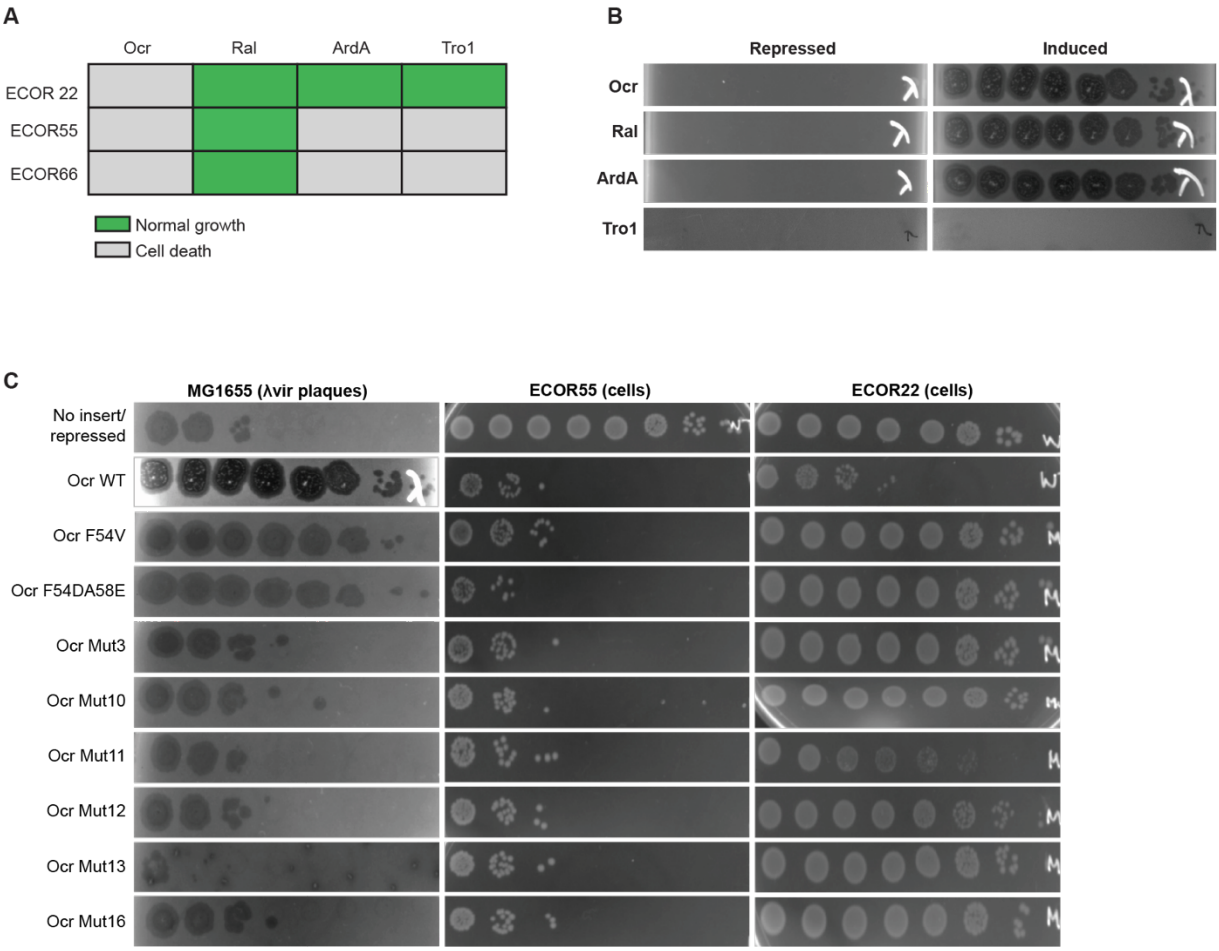


**Supplementary Figure 1. Conditional-lethal phenotypes of known R-M inhibitors in wild *E. coli*.** Related to Figures 2, 3. **(A)** Schematic representation of conditional-lethality data from Figure 3a, showing only known R-M inhibitors and an uncharacterized AG, *orf7* (*tro1*). **(B)** AGs from (A) tested for their ability to block EcoKI restriction of phage λvir in plaque assays with restriction-competent *E. coli* MG1655. **(C)** Various mutants of Ocr tested in MG1655 for their ability to block EcoKI restriction of λvir, and in ECOR22 and ECOR55 for their ability to trigger PCD activity of EcoR22I and Ronin respectively. Representative panels from triplicate experiments shown.

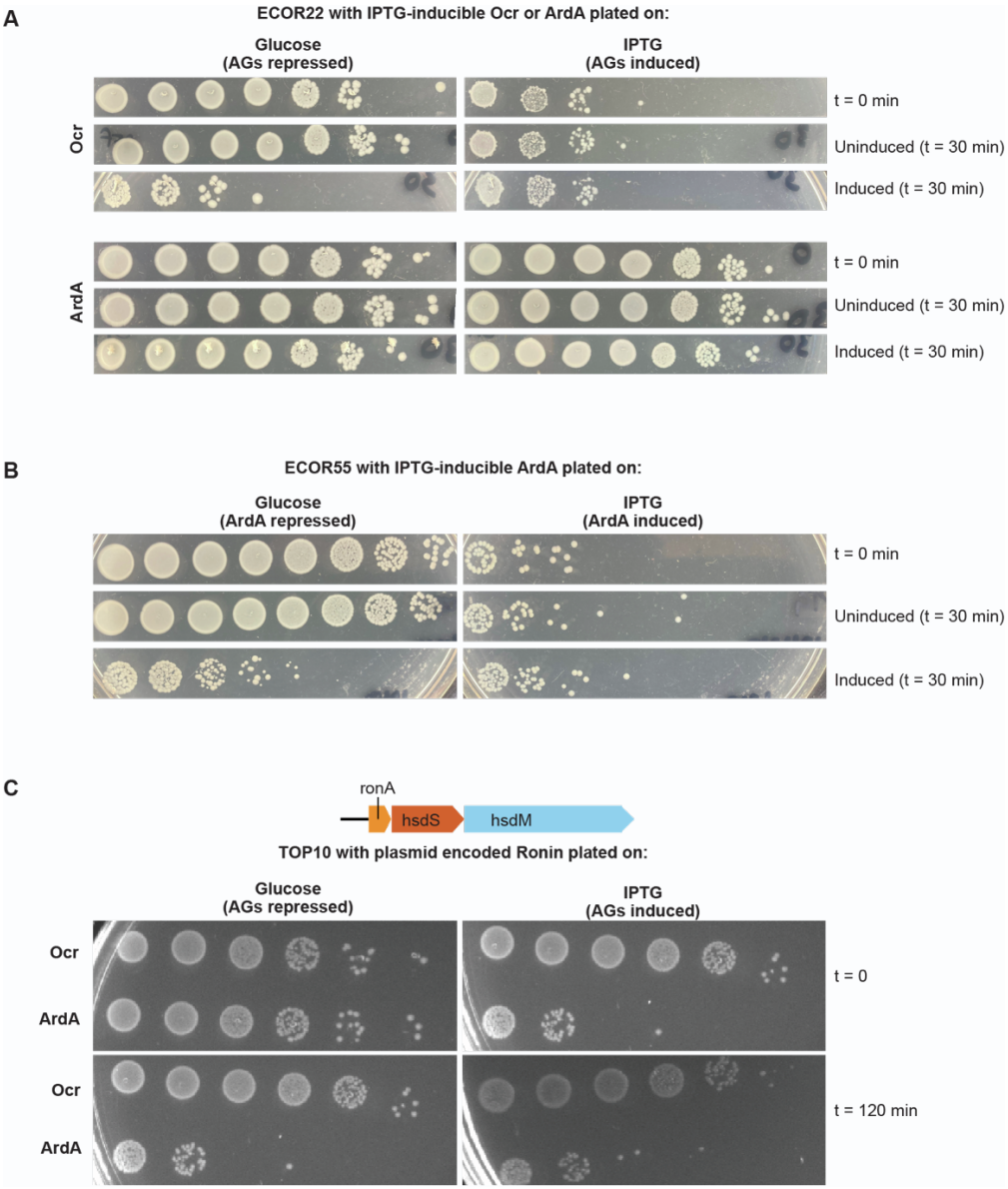


**Supplementary Figure 2. Irreversible cell killing by ECOR22I and Ronin.** Related to Figures 3, 4. **(A)** Ocr and ArdA were expressed transiently (liquid cultures incubated for 30 min with IPTG) in the wild strain ECOR22 and subsequently repressed by plating on Glucose-containing agar plates (or expressed continuously by plating on IPTG). Ten-fold serial dilutions of cultures plated before and after transient IPTG treatment. A parallel uninduced control (without any added IPTG in liquid culture) is also shown. Since Ocr triggers PCD by ECOR22I but ArdA does not (see Figure 2b), ArdA serves as a negative control for this experiment. **(B)** As in (A), but with transient expression of ArdA only in wild strain ECOR55 (since ArdA and Ocr both have the same PCD-triggering phenotype in ECOR55). **(C)** Cell killing upon transient expression of PCD-triggering AGs tested after reconstitution of Ronin in the TOP10 lab strain to take advantage of the fact that Ocr stops triggering Ronin in this configuration and can now serve as a negative control. The duration of transient expression of AGs was also extended to 120 min since full killing had not been achieved in (B) in 30 min (comparing the Induced sample plated on Glucose vs IPTG). Representative panels from triplicate experiments shown.

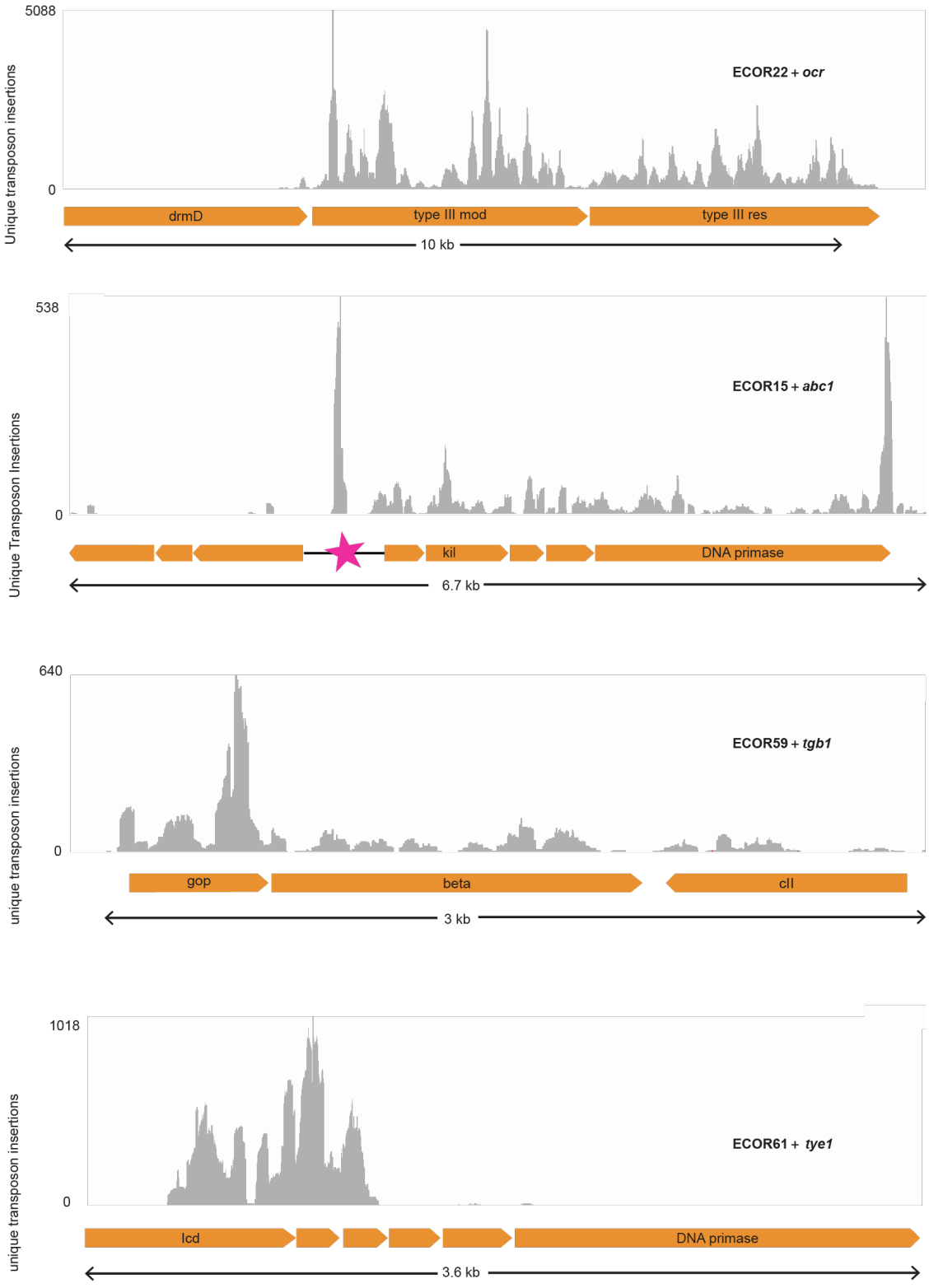


**Supplementary Figure 3. Transposon insertions that suppress AG-induced conditional-lethal phenotypes.** Related to Figures 3, 6. Distribution of unique transposon insertions recovered from survivors in Tn5 libraries upon trigger AG induction, mapped to each PCD locus in the respective ECOR strains.

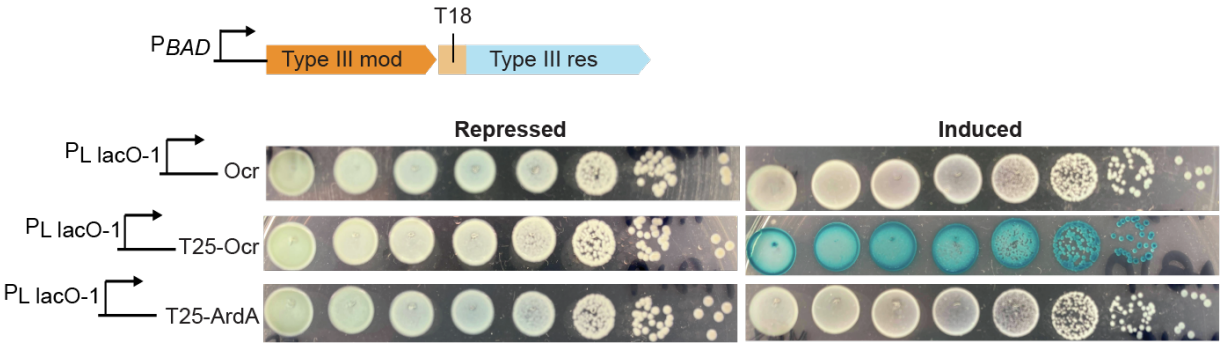


**Supplementary Figure 4. BACTH assay for direct physical interaction between Ocr and EcoR22I.** Related to Figure 3. As in Figure 3d, Bacterial Two-Hybrid (BACTH) assay with adenylate cyclase (AC) fragments T25 fused to the N-terminus of Ocr or ArdA and T18 fused to the the N-terminus of EcoR22I-Res. Blue staining results from hydrolysis of X-gal upon reconstitution of AC fragments, which stimulates production of the ß-galactosidase enzyme LacZ. Representative panels from triplicate experiments shown.

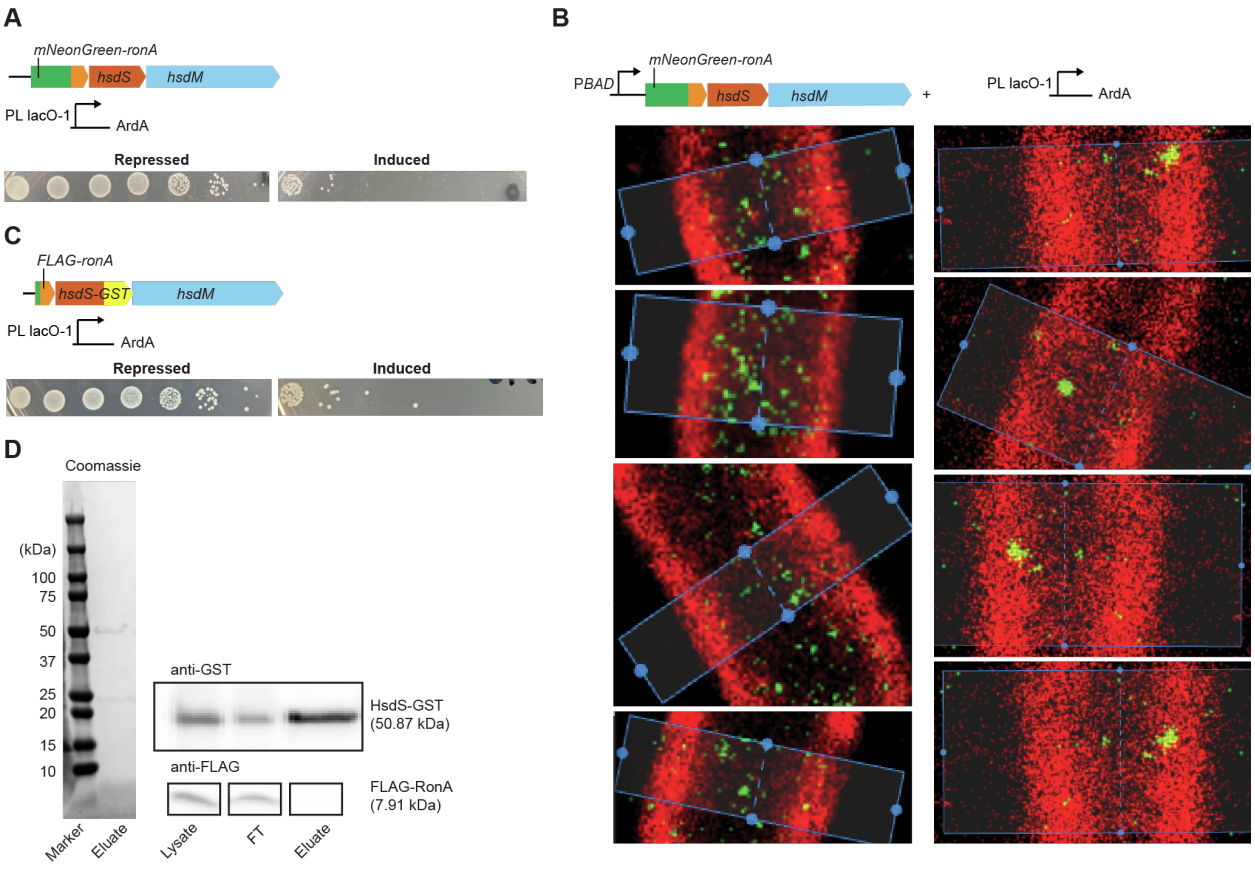


**Supplementary Figure 5. Tagging ronA and HsdS components of Ronin.** Related to Figures 4, 5. **(A)** Verification that the mNeonGreen-RonA fluorescently tagged Ronin construct is still active and can enact PCD upon ArdA expression (serial tenfold dilutions of saturated culture; ArdA repressed: top, induced: bottom). **(B)** Representative single-molecule super-resolution microscopy images used for quantification of mNG-RonA distributions in Figure 4h. mNG-RonA foci are observed at the cellular periphery upon overexpression of Ronin and ArdA (right), but not in cells without ArdA (left). **(C)** Verification that the FLAG-*ronA* and *hsdS*-GST dual tagged Ronin construct is still active (as in A). **(D)** Immunoprecipitation (IP) of HsdS-GST protein from cell lysates prepared from stationary-phase cultures of Ronin-expressing *E. coli*. Purified eluate after GST IP is analysed by SDS-PAGE and Coomassie staining next to a protein size marker, with a 50 kDa band corresponding to HsdS-GST fusion protein faintly visible. Western blots of the raw cell lysate, the flowthrough after incubation with Glutathione Sepharose beads, and the purified eluate (the same as in the Coomassie stained gel) are shown, upon probing either with an anti-GST or anti-FLAG antibody. Crop boundaries are shown with thick black outlines, and the HsdS-GST and FLAG-RonA bands are arranged relative to the ladder. Representative panels from triplicate experiments shown in A, C.

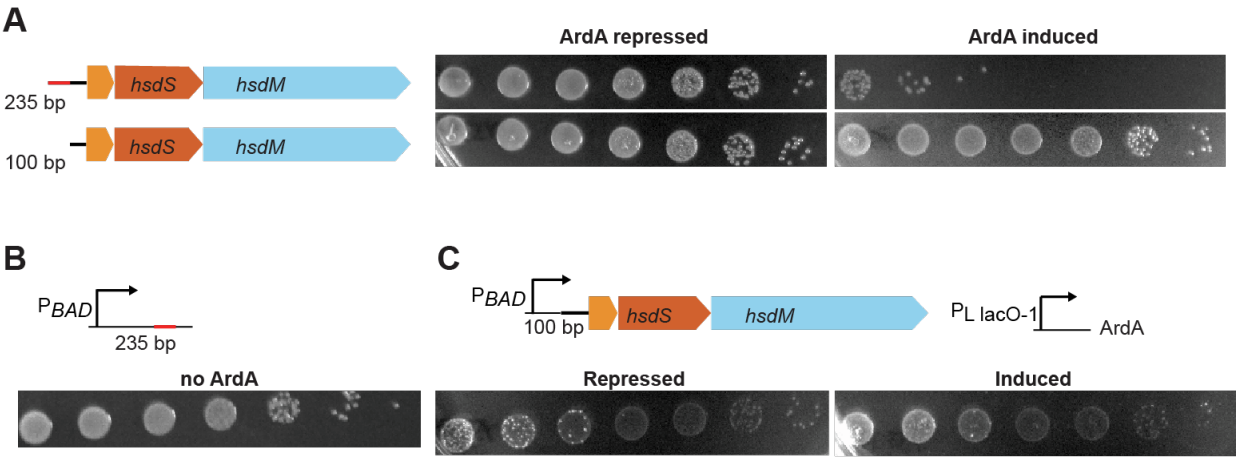


**Supplementary Figure 6. Upstream non-coding region is required for Ronin PCD activity.** Related to Figures 4, 5. **(A)** Truncation of the upstream non-coding region down to 100-bp causes Ronin inactivation. ArdA is chromosomally integrated under pLlacO-1 control and strains in the left (ArdA repressed) and right (ArdA induced) panels are isogenic. (serial tenfold dilutions of saturated culture) **(B)** Over-expression of 235-bp upstream region itself is not toxic in TOP10 indicating that it is not the PCD effector. **(C)** PCD phenotype of truncated Ronin system assayed as in (A), when the construct is overexpressed (indicated as "p*BAD*"). Representative panels from triplicate experiments shown.